Transportation Consortium of South-Central States

Solving Emerging Transportation Resiliency, Sustainability, and Economic Challenges through the Use of Innovative Materials and Construction Methods: From Research to Implementation

Reduction of Structural Damage from the Thermal Expansion of Concrete Using Multifunctional Materials

Project No. 18STTAM01

Lead University: Texas A&M University

Final Report

October 2019

Disclaimer

The contents of this report reflect the views of the authors, who are responsible for the facts and the accuracy of the information presented herein. This document is disseminated in the interest of information exchange. The report is funded, partially or entirely, by a grant from the U.S. Department of Transportation's University Transportation Centers Program. However, the U.S. Government assumes no liability for the contents or use thereof.

TECHNICAL DOCUMENTATION PAGE

1. Project No.	2. Government Accession No.	3. Recipient's Catalog No.
18STTAM01		

4. Title and Subtitle	5. Report Date
Reduction of Structural Damage from the Thermal Expansion of Concrete Using Multifunctional Materials	Oct. 2019
	6. Performing Organization Code
7. Author(s)	**8. Performing Organization Report No.**
PI: Darren Hartl https://orcid.org/0000-0001-9922-0481 Post-Doc: Mirmilad Mirsayar https://orcid.org/0000-0002-2006-4189	
9. Performing Organization Name and Address	**10. Work Unit No. (TRAIS)**
Transportation Consortium of South-Central States (Tran-SET) University Transportation Center for Region 6 3319 Patrick F. Taylor Hall, Louisiana State University, Baton Rouge, LA 70803	**11. Contract or Grant No.** 69A3551747106
12. Sponsoring Agency Name and Address	**13. Type of Report and Period Covered**
United States of America Department of Transportation Research and Innovative Technology Administration	Final Research Report Mar. 2018 – Mar. 2019
	14. Sponsoring Agency Code

15. Supplementary Notes

Report uploaded and accessible at Tran-SET's website (http://transet.lsu.edu/).

16. Abstract

This study leveraged past successes in the analysis and design of shape memory alloy (SMA) components to address the issue of thermal expansion in concrete structures. Since the SMA used in the current work is relatively cheaper than other common SMAs (less than $50/lb compared to NiTi which is $200/lb due to difficulties in processing), it is anticipated that the findings of the study could be implemented in real infrastructures made of concrete, asphalt concrete, and other complex large infrastructure. Low-cost Fe-SMAs and other multifunctional materials can be considered as a replacement for components made of steel (e.g., in reinforced or plain jointed concrete pavements) to control distresses resulting from thermal expansion during seasonal/daily temperature change. This study conducted a series of finite element (FE) case studies of various configurations of concrete (blocks, slabs, and beams) with embedded, pre-strained SMA rods. This included developing new models to investigate temperature induced deflection in concrete slabs to analyze their curling behavior. It also included investigating the optimal position of the SMA rod and required rod radius. It is hoped that the results of this work could help to design smarter civil infrastructure incorporating multifunctional materials into established civil engineering materials.

17. Key Words	18. Distribution Statement
Shape memory alloys, Fe-SMA rod, Structural optimization, Thermal expansion, Multifunctional materials, Concrete curling	No restrictions. This document is available through the National Technical Information Service, Springfield, VA 22161.

19. Security Classif. (of this report)	20. Security Classif. (of this page)	21. No. of Pages	22. Price
Unclassified	Unclassified	34	

Form DOT F 1700.7 (8-72) **Reproduction of completed page authorized.**

SI* (MODERN METRIC) CONVERSION FACTORS

APPROXIMATE CONVERSIONS TO SI UNITS

Symbol	When You Know	Multiply By	To Find	Symbol
		LENGTH		
in	inches	25.4	millimeters	mm
ft	feet	0.305	meters	m
yd	yards	0.914	meters	m
mi	miles	1.61	kilometers	km
		AREA		
in^2	square inches	645.2	square millimeters	mm^2
ft^2	square feet	0.093	square meters	m^2
yd^2	square yard	0.836	square meters	m^2
ac	acres	0.405	hectares	ha
mi^2	square miles	2.59	square kilometers	km^2
		VOLUME		
fl oz	fluid ounces	29.57	milliliters	mL
gal	gallons	3.785	liters	L
ft^3	cubic feet	0.028	cubic meters	m^3
yd^3	cubic yards	0.765	cubic meters	m^3
		NOTE: volumes greater than 1000 L shall be shown in m^3		
		MASS		
oz	ounces	28.35	grams	g
lb	pounds	0.454	kilograms	kg
T	short tons (2000 lb)	0.907	megagrams (or "metric ton")	Mg (or "t")
		TEMPERATURE (exact degrees)		
^oF	Fahrenheit	5 (F-32)/9 or (F-32)/1.8	Celsius	^oC
		ILLUMINATION		
fc	foot-candles	10.76	lux	lx
fl	foot-Lamberts	3.426	$candela/m^2$	cd/m^2
		FORCE and PRESSURE or STRESS		
lbf	poundforce	4.45	newtons	N
lbf/in^2	poundforce per square inch	6.89	kilopascals	kPa

APPROXIMATE CONVERSIONS FROM SI UNITS

Symbol	When You Know	Multiply By	To Find	Symbol
		LENGTH		
mm	millimeters	0.039	inches	in
m	meters	3.28	feet	ft
m	meters	1.09	yards	yd
km	kilometers	0.621	miles	mi
		AREA		
mm^2	square millimeters	0.0016	square inches	in^2
m^2	square meters	10.764	square feet	ft^2
m^2	square meters	1.195	square yards	yd^2
ha	hectares	2.47	acres	ac
km^2	square kilometers	0.386	square miles	mi^2
		VOLUME		
mL	milliliters	0.034	fluid ounces	fl oz
L	liters	0.264	gallons	gal
m^3	cubic meters	35.314	cubic feet	ft^3
m^3	cubic meters	1.307	cubic yards	yd^3
		MASS		
g	grams	0.035	ounces	oz
kg	kilograms	2.202	pounds	lb
Mg (or "t")	megagrams (or "metric ton")	1.103	short tons (2000 lb)	T
		TEMPERATURE (exact degrees)		
^oC	Celsius	1.8C+32	Fahrenheit	^oF
		ILLUMINATION		
lx	lux	0.0929	foot-candles	fc
cd/m^2	$candela/m^2$	0.2919	foot-Lamberts	fl
		FORCE and PRESSURE or STRESS		
N	newtons	0.225	poundforce	lbf
kPa	kilopascals	0.145	poundforce per square inch	lbf/in^2

TABLE OF CONTENTS

LIST OF FIGURES

LIST OF TABLES

ACRONYMS, ABBREVIATIONS, AND SYMBOLS

FEA	Finite Element Analysis
MSMA	Magnetic Shape Memory Alloy
SMA	Shape Memory Alloy

EXECUTIVE SUMMARY

Control of thermal expansion is a critical goal of engineering design in a wide range of applications, particularly in cases where system components are small, are subject to large changes (gradients) in temperatures, or require extreme dimensional stability over a wide range of temperatures. Thermal expansion causes thermal stresses in structures and structural failure can happen as a result of excessive thermal strains. In structures made of brittle materials (e.g., concrete), stresses induced by the thermal expansion would lead to the catastrophic structural failure. Thermal expansion compensation often requires materials with either negative or (close to) zero thermal expansion. Because of the thermomechanical coupling behavior, shape memory alloys are one of the best candidates for this purpose. The most common SMA candidate for such applications is the NiTi SMA, which is expensive for civil infrastructures due to large scale applications. For such reasons, we can replace NiTi SMA with iron-based SMA which is low-cost and can be processed easily, compared to NiTi SMA, to address the issue of thermal expansion. However, integrating such high performance materials into next generation designs is challenging since systems and materials that address the problem of thermal expansion must not significantly increase the overall complexity of the current infrastructure and must be scalable so that they may be implemented in a variety of structural configurations. Materials with passive actuation based on changes in temperature could be used to counter the damage caused by thermal expansion. Solutions that incorporate design optimization and adaptive, durable materials are of particular interest.

As a result, this work proposes to leverage past successes in the analysis and design of shape memory components to address the issue of thermal expansion in concrete structures. It is hoped that the results of this work could help to design smarter civil infrastructures incorporating multifunctional materials into the old civil engineering material. Since the SMA used in the current work is relatively cheaper than other common SMAs (less than $50/lb compared to NiTi which is about $200/lb due to difficulties in processing), it is anticipated that the findings of the current research could be implemented in real infrastructures made of concrete, asphalt concrete, and other complex large infrastructures. However, the focus of the current research would be on concrete infrastructures and the applicability of the findings to the infrastructures made of other civil engineering materials can be explored later on. For the applications considered, low-cost Fe-SMAs and other multifunctional materials can be considered as a replacement for components made of steel (e.g., in reinforced or plain jointed concrete pavements) to control distresses resulting from thermal expansion during seasonal/daily temperature change. It should be noted there are potential approaches to reduce cost in competing SMAs, but FeSMAs are an order of magnitude cheaper than traditional SMAs (e.g., NiTi). Through a combined approach of structural optimization, mechanics, and materials design, this research aims at simultaneously achieving advantageous mechanical properties and passive actuation behavior in a single material for concrete infrastructures. Curling in concrete slabs due to the time-dependent temperature gradient through the slab thickness is considered as the specific problem to solve. The project will define a viable path for technology transfer by establishing substantive partnerships with commercial alloy manufacturers, and cultivate the awareness and expertise in the technology through workforce development and outreach activities.

1. INTRODUCTION

Thermal expansion is inevitable during the service life of transportation infrastructure, either due to the seasonal or daily temperature changes, often resulting in structural damage and expensive design modifications. Thermal expansion of concrete structures causes misalignment, cracking, and structural failure. Curling of the concrete slabs due to the temperature gradient throughout the slab thickness is a well-known example of distresses in transportation infrastructures due to thermal expansion *(1)*. As a result, innovative solutions and strategies are needed to mitigate damage caused by the thermal expansion of transportation infrastructure. To enhance the longevity and safety of these structures, high-performance materials that address the issue of thermal expansion must be integrated into next generation designs. Improvements in materials and advances in computing and control technology make it possible to apply sophisticated active control technology to civil engineering structures *(2, 3)*. Shape memory alloys (SMAs) are one of the so-called "smart" or "multifunctional" materials. From a macroscopic point of view, the observable mechanical behavior of shape memory alloys can be separated into two major categories: one is the shape memory effect (SME), in which a specimen exhibits a larger residual strain after loading and unloading that can be fully recovered upon raising the temperature of the material; the other is the pseudoelasticity, in which a specimen achieves a very large strain upon loading that is then fully recovered in a hysteresis loop upon unloading. Regarding the shape memory effect of SMA, the amount of recovery depends on the activation temperature, the initial deformation, and the percentage of marstensite phase that is present in the material. The recovery properties have led to many applications of SMAs as activated actuators. SMA has been proposed for large strain actuators for use in smart structures. The interesting properties of SMAs have inspired the research of possible applications of these alloys in the field of civil engineering *(4–17)*. Such applications include shape and active vibration control and acoustic control with a shape memory alloy wire or layer *(4)*, the active control of electrometric rods with embedded two-way shape memory alloy actuators *(6)*, a base isolation system with a shape memory alloy device that is based on the pseudoelastic effect for elevated highway bridges *(8)*, a structure's seismic isolation *(10, 11)*, and a shape memory alloy damper for the structural control *(15–17)*.

Currently, the most common SMA candidate for such applications is the NiTi-based alloy also known as "Nitinol". While it shows excellent superelastic properties, the high cost due to inherent materials cost, difficulty in processing and fabrication, and limited in supply severely limit its application in largescale applications in transportation projects. Therefore, there is a need for an alternative to Nitinol that is cost-effective, easily processed, and show comparable superelastic response. Due to relatively low costs for alloying elements and good workability compared to conventional shape memory alloys (SMAs), iron-based SMAs have attracted considerable attention in the last decade *(18–23)*. In recent years, a FeMnAlNi SMA showing large full-recoverable superelasticity and high strength was engineered that could address this need *(21-23)*. This Fe-SMA contains inexpensive alloy elements and does not require high vacuum during melting required for titanium-based alloys like NiTi.

The thermal expansion behavior of SMAs has been explored by some researchers in the past, in order to control thermal strains in structures subjected to large temperature changes *(24–26)*. As an interesting effort, it has been shown recently that through thermomechanical processing, it is possible to tailor the thermal expansion of SMAs, without manipulating their compositions, over a wide range of positive and negative values *(24)*. The issue of controlling thermal expansion in infrastructures by the use of SMAs has not been investigated seriously due to the cost inefficiency

of using common SMAs (e.g., Nitinol). However, utilizing low-cost Fe-based SMAs, it is aimed in this research to investigate the possibility of controlling thermal expansion in concrete infrastructures in order to reduce structural damage. Systems and materials that address the problem of thermal expansion must not significantly increase the overall complexity of the current infrastructure and must be scalable so that they may be implemented in a variety of structural configurations. Materials with passive actuation based on changes in the temperature could be used to counter the damage caused by thermal expansion. Solutions that incorporate design optimization and adaptive, durable materials are of particular interest. Indeed, a detailed numerical simulation together with experimental efforts could reveal the efficiency of utilizing SMAs as a thermal expansion controller in concrete structures.

2. OBJECTIVES

The global objective of this research is to improve durability and extending the life of the transportation infrastructure using multifunctional materials. Thermal expansion of concrete plays a significant role in the durability of the transportation infrastructure and causes misalignment, cracking, and structural failure. This research is aimed to use high-performance materials that address the issue of thermal expansion integrated into next generation designs, to enhance the longevity and safety of these structures. As a result, the more specific objective of this research is to design and characterize the use of multifunctional materials that stabilize the changing structure due to thermal expansion. The characteristics of these materials will work in conjunction with the temperature dependence of concrete. This will require very specific properties from the materials, making trained shape memory alloys (SMA's) a likely candidate, to meet the characteristics required to address the problem statement. The methods to train the materials should be developed in a repeatable fashion, and their adaptability demonstrated as a function of temperature and stress from the thermal expansion of the concrete.

In summary, the research should address the following research tasks:

1. Design and characterization of multifunctional materials for reduction of structural damage from the thermal expansion;
2. Optimization of the topology and configuration of these materials in infrastructures to improve the structural performance against thermally induced distresses; and
3. Demonstration of capabilities of the approach in a realistic infrastructure system.

3. LITERATURE REVIEW

3.1. Rigid Pavements

Based on the structural performance, pavements can be classified into two categories: flexible pavements and rigid pavements. In flexible pavements, wheel loads are transferred by grain-to-grain contact of the aggregate through the granular structure. Since they are made of bituminous materials and aggregates, the flexural strength of the flexible pavements is less and they behave like a flexible plate. On the contrary, in rigid pavements which are made of cementitious materials and aggregates, wheel loads are transferred to sub-grade soil by flexural strength of the pavement and the pavement behaves like a rigid sheet. In the current study, we concentrate on rigid pavements which are used in many countries all around the world. Rigid pavements are made up of Portland cement concrete, and may or may not have a base course between the pavement and the subgrade. Rigid pavements tend to distribute the load over a relatively wide area of subgrade, and as a result, the major portion of the structural capacity is supplied by the concrete slab itself. They can be used for heavier traffic loads and can be constructed over relatively poor subgrade.

There are four types of rigid pavements: Jointed plain concrete (JPC) pavement, jointed reinforced concrete (JRC) pavement, continuously reinforced concrete (CRC) pavement, and pre-stressed (PC) concrete pavement. JPC Pavements are plain cement concrete pavements constructed with closely spaced contraction joints. Dowel bars or aggregate interlocks are usually employed for load transfer across pavement joints (joint spacing usually varies from 5 to 10m). In JRC, the reinforcements do not significantly improve the structural capacity, but can drastically increase the joint spacing (10 to 30m). Dowel bars are also used as load transfer in JRC pavements. CRC pavements are Portland cement concrete pavement with continuous longitudinal steel reinforcement and no intermediate transverse expansion or contraction joints. Instead, the pavement is allowed to crack in a random pattern and the cracks are held tightly closed by the steel reinforcement. As shown in Figure 1, in this research we particularly focus on models for prediction of the displacements in reinforced concrete pavements (e.g., CRCP) rather than unreinforced types.

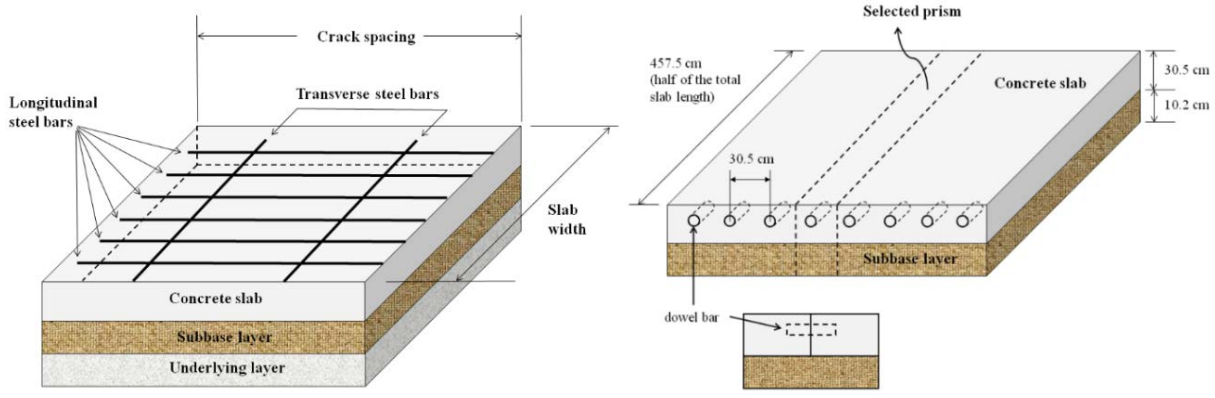

Figure 1. General configuration of (a) CRC pavement and (b) JPC pavement with typical dimensions.

The first use of CRC pavements was in 1921 by the Bureau of Public Roads on Columbia Pike in Arlington, Virginia. Then, the first significant length of CRC pavements was constructed in the State of Indiana in 1938 *(27)*. After that, good performance of such projects (like the one in Illinois,

California, and New Jersey around 1949) led to an increased interest in this design *(28)*. The use of CRC pavements was increased in the 1960s, 1970s, and 1980s during construction of the Interstate Highway System in the U.S. The use of CRC pavements in the U.S. was increased for more than 15,000 kilometers of equivalent two-lane pavement were in use or under contract at the end of 1971 *(27)* and this amount is still increasing. Texas and Illinois, with dissimilar weather and environmental conditions, lead the nation in CRCP usage. Texas constructed its first section in Ft. Worth in 1951. From the 1960s on, Texas has constructed more CRC pavements than any other state, possibly more than all other states combined. Approximately 80 percent of current concrete paving projects let in Texas are CRC pavements. Illinois constructed its first CRC pavement in 1947 on U.S. 40 west of Vandalia. Based on the performance of this experimental project, Illinois began extensive construction of CRC pavements. Approximately two-thirds of the Illinois Interstate system was constructed with CRC pavements *(29)*.

3.2. Factors affecting Displacements in Concrete Slabs

There are many factors influencing displacements in concrete pavements. Among them, we can mention temperature, moisture, material properties of the slab and subbase, bond behavior between slab and subbase, and the location and radius of the steel bar in CRC pavements. Particularly, as one of the major sources, we are interested in temperature and material properties effects in the current research following the original goal of the current study which is controlling the thermal expansion with tailorable material properties of multifunctional materials.

3.2.1. Temperature of the Concrete Slab

One of the primary sources of the stress in concrete slabs is thermal stress. In concrete pavements, the thermal stress depends on: (1) the thermal properties in early ages which can be often characterized as heat of hydration and coefficient of thermal expansion, (2) the conditions at placement, (3) the environmental effects (ambient air temperature and solar radiations), and (4) geometry of the structure. The thermal stress field in concrete slabs is influenced by the boundary conditions of the slab. If a concrete slab is unrestrained, it expands and contracts during the early-age heating and the subsequent cooling process without stress development. However, concrete slabs are always restrained to some degree, either externally by adjoining structures or internally by different temperature in the components of the structure itself. Therefore, due to such imposed restraint conditions, temperature change results in compressive and/or tensile stresses in the concrete. Thus, a primary question would be, whether the induced thermal stresses lead to cracking or not *(30)*.

Due to the hydration of the fresh concrete, energy releases in the form of heat. Mixing Portland cement compounds with water leads to a rapid release of heat initially, which then drops down within about 10 to 20 minutes. This reaction probably represents the heat of the solution of sulfates and aluminates in the mixture *(31)*. The primary heat generation cycle starts a couple of hours after the cement compounds are mixed with water. Before that, concrete is in a plastic state and is relatively inactive chemically. A couple of hours after concrete is mixed with water, the peak of the primary cycle reaches its peak value. At this step, the major portion of the hydration products crystallizes from the solution of the mixture. This step includes the time of the initial and/or final set of the concrete. As hydration products grow, they form a barrier to the infiltration of additional water; and when there is no room for further growth of crystals, or when hydration is theoretically completed the reaction drops down and may eventually stop *(29, 32)*. The rate of hydration is very

sensitive to temperature, especially during the primary cycle *(29, 32)*. Therefore, the temperature condition during construction is an important factor affecting the rate of hydration.

Most importantly, environmental conditions lead to temperature gradients in concrete slabs. The high temperature in fresh concrete due to ambient air temperature and solar radiation may induce such undesirable effects as increased water demand, increased rate of setting, increased rate of slump loss, difficulties in controlling entrained air, increased tendency for plastic shrinkage cracking, and the critical need for prompt curing *(29)*. In hardened concrete, high temperature may lead to decreased strength, increased shrinkage, increased creep, decreased durability, and non-uniformity of surface *(33, 34)*. Also, because the hydration of cement is a chemical process, high ambient temperature will increase the rate at which the concrete hydrates. High solar radiation during construction may also significantly influence on increasing the concrete temperature as well as the rate of hydration. This expedited rate of hydration results in a higher and earlier peak concrete temperature during the construction day *(35)*. The coefficient of thermal expansion (COTE) is also a key parameter affecting on the thermal stress distribution in concrete slabs. Like all composite materials, the COTE of concrete is influenced by a large number of factors that can be generally related to its major components: cement paste and aggregate. Primarily affected by the moisture content of the paste, the COTE of the paste vary significantly during the hydration process and will be stabilized thereafter. The thermal characteristics of concrete obviously affect the crack pattern in concrete slabs since thermally induced dimensional changes in the Portland cement concrete influence the formation of transverse cracks. The type of coarse aggregate also directly influences on COTE of concrete, because coarse aggregates form a large part of concrete by volume *(36)*.

3.2.2. Material Properties

The material properties of the concrete slab, subbase layer, and reinforcing steel significantly influence displacements in pavement structures. For concrete slab, the material properties of the concrete ingredients (cement paste and aggregates) represents the effective modulus of the concrete. The stiffness and strength of each component influences crack pattern in a concrete slab and therefore are essential to be studied. The stiffness of each layer in a concrete pavement structure directly relates to the overall displacements in the structure. The effect of stiffness of layers on the displacement field in concrete slabs has been investigated by the researchers in the past *(37–39)*. In the previous researches, the concrete slab and base layer are modeled as linear elastic plates connected by springs (Winkler foundation) and the displacements in the pavement is evaluated by plate theories (like Mindlin plate theory). However, the concept of using springs as interface elements brings many problems since such spring models does not represent de-bonding mechanism between layers in a sophisticated manner. The displacements in the concrete slab are developed in either elastic deformations or de-bonding (permanent deformations). To fill this gap, a sophisticated model representing both de-bonding and elastic deflections has been developed by employing theoretical and computational fracture mechanics techniques through an extensive two-dimensional finite element analysis *(1)*.

3.3. Thermal Expansion in Concrete Infrastructure

Joints between concrete slabs provide a pathway that allows water from the surface to seep into, and weaken, the supporting base courses. In addition, they present a maintenance problem if the seepage is to be kept minimal since they must be resealed every few years. The joints also have an

adverse effect on the riding quality of the entire pavement and can be a source of driving discomfort *(40, 41)*. CRCP, shown in Figure 1a, was developed as an alternative to the jointed concrete pavement that eliminates the need for contraction joints. In CRCP, the longitudinal reinforcement is continuous, in that each individual length of reinforcing bar is welded or lapped end-to-end to each of its adjoining reinforcing bars in the reinforcement grid. The presence of steel in the pavement does not prevent the formation of cracks. Rather, it induces the concrete to develop numerous transverse, hairline cracks. Theoretically, the steel keeps the cracks tightly closed, which maintains the integrity of the aggregate interlock across the cracks. This prevents the formation of high shear stresses in the steel due to traffic loads and blocks the passage of water from the surface to the subgrade *(40)*.

In a pavement structure, with respect to temperature, when the slab surface is cooler than the slab bottom, the surface tends to contract and curling the slab edges (or corners) upward as a result of negative temperature gradient through the slab thickness. Lift-off (the separation of the slab from the subbase layer) is the first step towards erosion damage which is a distress type that threatens the sustainability of the concrete pavement. In a concrete slab, the lift-off is controlled by the net climatically induced contraction strain field, which takes into account both temperature and the moisture effects, the bond behavior between concrete slab and subbase, and the weight of the concrete slab. Such interaction causes a stress field throughout the slab which results in separation of the slab from the subbase. During lift-off, the temperature change has the first-order effects and the impact of the other parameters (e.g., humidity) are negligible *(41–43)*. Lift-off is the first step towards erosion damage which is a distress type that threatens the sustainability of the concrete pavement. A two-dimensional configuration of the slab displacements is shown in Figure 2. As shown, both shrinkage and thermal expansion/contraction affect the horizontal displacements while the vertical component (lift-off) is mostly affected by thermal strains.

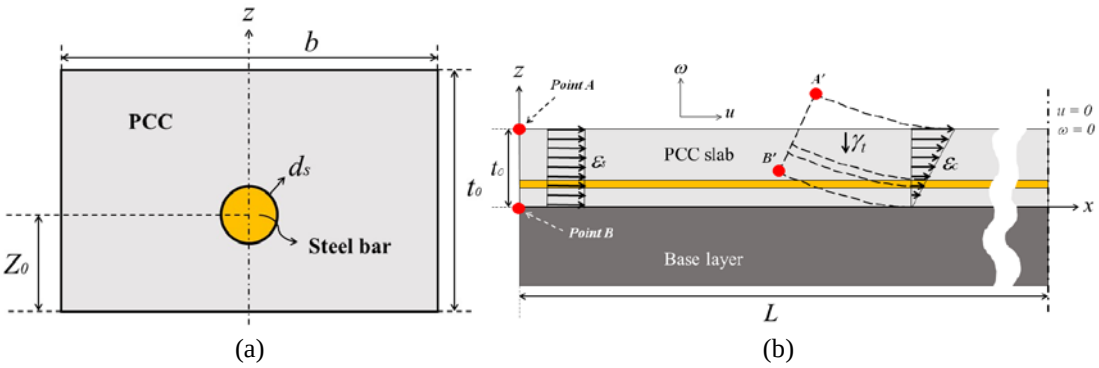

Figure 2. 2D scheme of the end movement in concrete pavements.

Both seasonal and daily temperature change could affect vertical end movements in concrete slabs. Figure 3(a) shows a typical temperature change in a concrete slab over Initial 7 Days after placement. Such a large temperature change could result in a large vertical displacements at different locations of the concrete slab, as shown in Figure 3(b). Due to the traffic load, areas affected by such vertical movements are subjected to bending moment causing structural cracking, as shown in Figure 4.

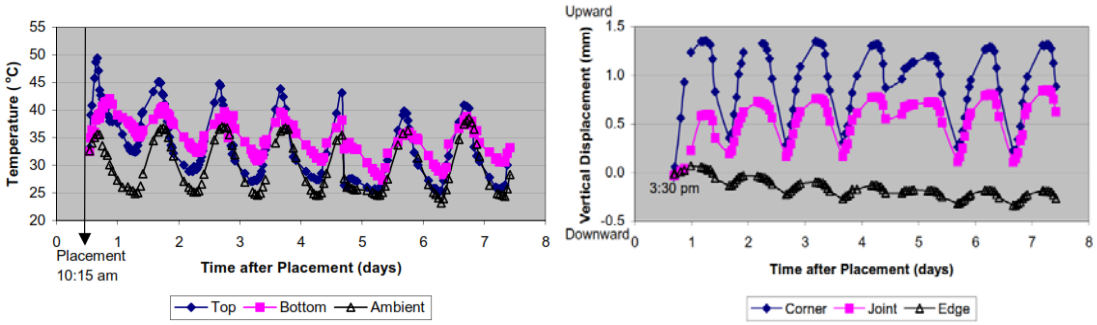

(a) (b)

Figure 3. Temperature change and vertical displacements of slab over Initial 7 Days *(43)*.

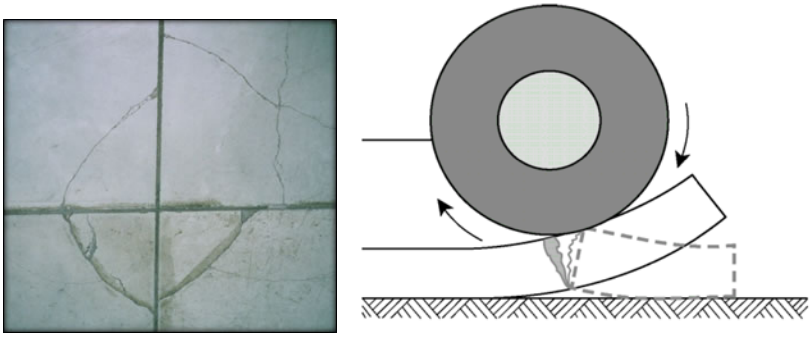

Figure 4. Cracking of the concrete slab corners due to lift-off and passing traffic load.

Due to such common distresses in concrete pavements, there is a need for controlling thermal expansion in concrete slabs. In addition to the major problems discussed above, concrete/ steel corrosion is another issue that happens, specifically at the joints. Such existing problems motivate us for conducting this research in order to find solutions by employing low-cost multifunctional materials.

3.4. Iron-Based Shape Memory Alloys

Shape memory alloys (SMAs) are a class of multi-functional materials that alter their crystallographic state from austenite to a martensite phase given appropriate stress or temperature stimuli, leading to large and ultimately recoverable strains and the alteration of a number of physical properties. Currently, the most widespread SMA are based on NiTi, or “nitinol”. While they show excellent superelastic properties, their high cost severely limits their application in large-scale applications in transportation projects. Recently, inexpensive FeMnAlNi SMA has been developed showing large full-recoverable superelasticity and high strength. Specifically, the recent introduction of a magnetic $Fe_{43.5}Mn_{34}Al_{15}Ni_{7.5}$ (FMAN) SMA *(21, 44–47)* has provided a solution to the poor loadbearing capabilities in magnetic shape memory alloys (MSMAs). This material demonstrates a combination of meta-magnetic shape memory effect and robust mechanical properties suitable for structural applications. It has been shown that the material can be produced in polycrystalline form and its tensile strength can exceed 800 MPa with a ductility of 10% strain, making it as one of the first MSMAs capable of exhibiting simultaneous self-sensing and self-centering when applied in an infrastructure system *(21)*. Of particular interest of the FMAN alloy is that superelasticity is observed in a wide temperature range from -196 to 200°C *(21)*. This property is crucial for the practical use of such materials in infrastructures since the self-

centering capabilities of the material will remain unaffected by the ambient temperature, and the technology can be used without modifications in both very hot and very cold climates.

Through a combination of precipitation hardening and grain size control techniques *(45, 48)*, it has been demonstrated that high-strength FMAN polycrystalline wires show large and fully reversible superelastic strains near 7%. Figure 5 shows the stress-strain response of an FMAN wire with 24-hour precipitation heat treatment at 200 °C. Compared to a conventionally processed nickel-rich NiTi superelastic alloy, the FMAN SMA shows a similar strength level and comparable level of transformation strain and energy dissipation (stress hysteresis) while exhibiting somewhat higher initial stiffness. On the other hand, both FMAN and NiTi are significantly stronger than CuAlMn SMAs, and possess the ability to dissipate a larger amount of energy per cycle. It is worth noting that the transformation stress level of the FMAN SMA can be easily increased or decreased by changing the duration of the precipitation heat treatment at 200 °C. For example, the 24 hour heat treated case shown in Figure 3 produces a high transformation the stress of 520 MPa. However, a lower transformation level may be desired in order to allow the self-centering response to trigger at lower deformation levels, for example, where a transformation stress level of 400 MPa is obtained when the heat treatment at 200 °C is shortened to 3 hours.

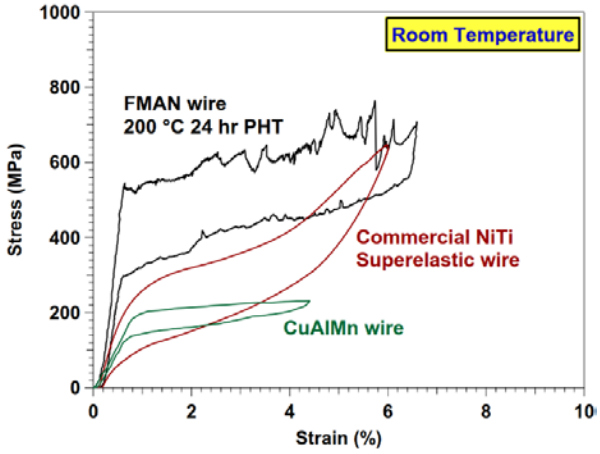

Figure 5. Comparison of the superelastic response of a FMAN wire with a conventional NiTi and a CuAlMn SMA.

4. METHODOLOGY

4.1. Modeling Approach

With the development of the high-speed digital computers, the use of finite element approaches in the design of concrete pavements has significantly been increased over the past decade *(49–51)*. Using the finite element method (FEM), one can simulate a pavement structure in any geometry and material properties under any loading profiles and boundary conditions. Such abilities of FEM can provide a more realistic understanding of the critical aspects of pavements response, such as joint load transfer, pavement response under traffic and environmental loads, and concrete slab/ subbase bond strength, that couldn't have been captured with other analytical solutions in a sophisticated manner. Many of the analytical solutions suggested in the past requires some sort of assumptions which may result in significant errors in prediction of the stresses, strains, and displacements in pavement structures. In the FEM, instead of solving the problem for the entire body in one operation, the formulation of the algebraic equations for each smaller bodies or units (finite elements) interconnected at points and the combination of equations yields the solution of a total structure. Although the solution obtained by the FEM is an approximation, it is possible to enhance the accuracy of the result by defining finer elements and providing accurate material properties. However one of the problems in using the commercial 3D FE software for rigid pavement modeling is that very few models have been validated and the various features of the software are not readily understood by the pavement designers. In other words, pavement engineers still are more comfortable in using other commercial programs which are specified for rigid pavements such as MEPDG, ISLAB, and EverFE to investigate the effects of temperature and moisture gradients, slab's modulus, and slab's dimensions.

There are many factors affecting the end movements in concrete pavements. Among them, slab dimensions, environmental loads (temperature and moisture gradients), and slab modulus are extensively investigated by the researches in the past decades using either analytical models or special-purpose programs. This section is dedicated to the modeling approach employed in the current analysis. The commercial finite element software ABAQUS *(52)* is utilized in the current research. A user material subroutine, developed in *(53)*, is implemented into ABAQUS to simulate the thermomechanical response of SMA bars embedded in the concrete structure. To results are obtained for the embedded reinforcing bars made of both steel and SMAs and compared and discussed. The results of the current research provide researchers with some insight as to the effect of different design parameters in controlling thermal expansion in concrete structures utilizing multifunctional materials and answer some of the primary questions on the use of such materials in the next generation of the smart infrastructures.

Figure 6 shows a prism taken out of the middle of the edge of a typical CRCP structure in order to phenomenologically investigate temperature-induced end movements in concrete slabs. The deformation at the corners can be simulated by applying the corresponding boundary conditions. It is found that all dimensions shown in Figure 6 can play significant roles in the end displacements of the slab *(42)*. Surface-to-surface cohesive zone approach *(1)* is used to connect concrete slab and subbase layer, as well as the concrete slab and the reinforcing steel bar.

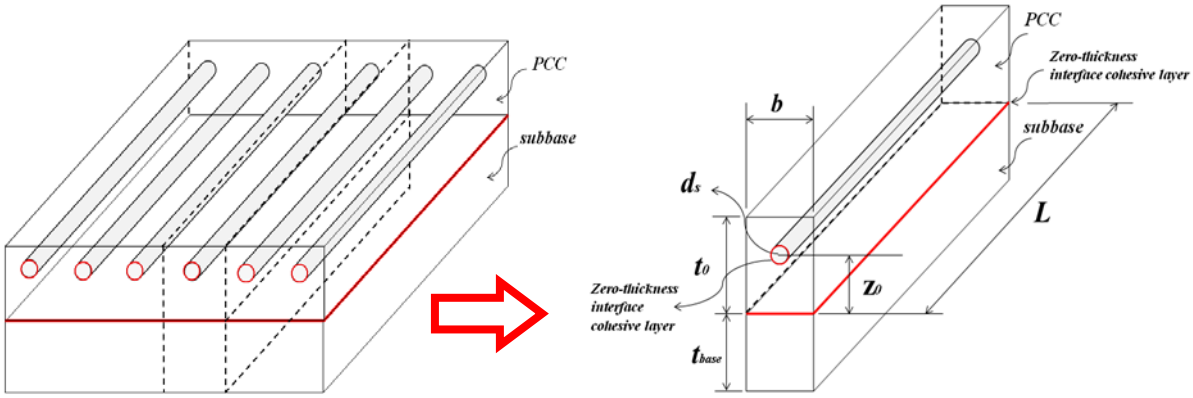

Figure 6. Geometry of the CRCP structure used for the three-dimensional finite element simulations.

As preliminary results, the CRCP prism with reinforcing "steel" bars is simulated for different linear temperature gradients from slab's bottom (point B) to the slab's top (point A), as shown in Figure 7. Vertical and horizontal displacements are tracked at three points of the slab edge: A) top of the slab, B) bottom of the slab, and C) at the interface of reinforcing steel bar and concrete slab. Since the reinforcing steel bar is restricted at its end, the horizontal displacement at point C roughly represents the bond slip between the concrete and the reinforcing steel bar. The bond strength between the concrete slab and the reinforcing bar is assumed to be a constant value of 5MPa *(42)*, and steel bar #6 (ds = 0.75in = 1.905cm) was used for all simulations.

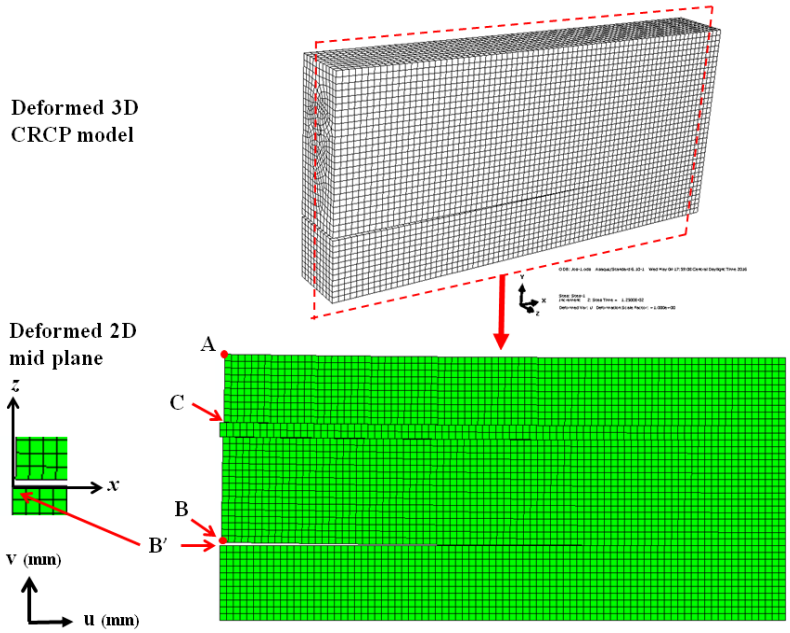

Figure 7. Mesh pattern for deformed CRCP, as well as the deformed mid plane *(42)*.

With fixed dimensions and material properties, the effects of temperature drop (which can be considered as a daily/ seasonal temperature changes) are obtained on horizontal and vertical displacements and points A, B, and C. It is seen from Figure 8 (a, b), that both horizontal and vertical displacements are dramatically influenced by the temperature gradient throughout the concrete thickness. The end movement in CRC pavement increases as the temperature difference

increases. It should be noted that Figure 8 is obtained for the nighttime temperature conditions in which the top surface of the slab is cooler than its bottom surface. However, the nighttime temperature profile is chosen since upward curling occurs under such conditions.

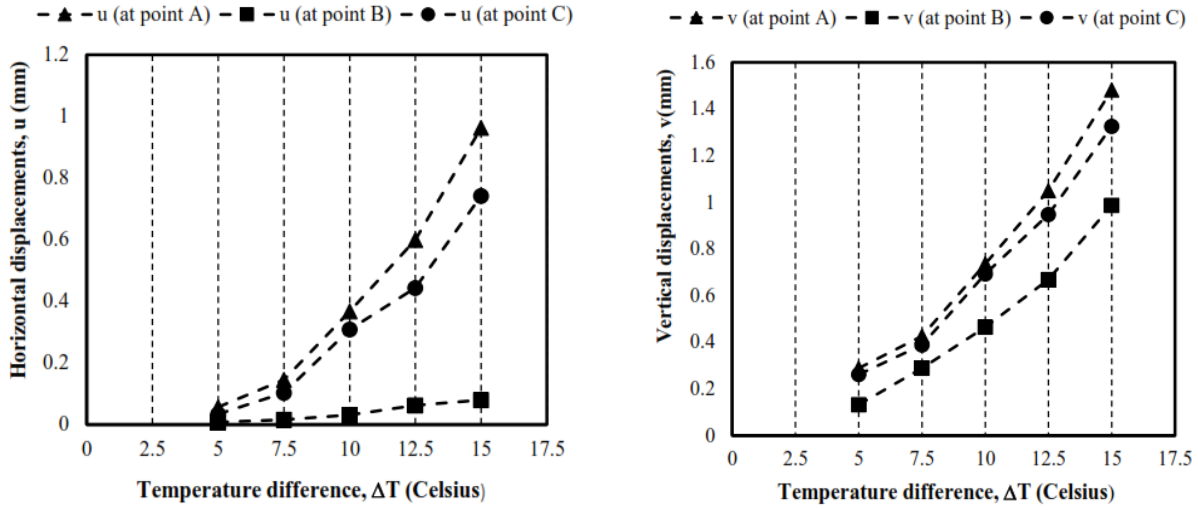

(a) (b)

Figure 8. Variation of displacements at the slab edge versus different temperature differences: (a) horizontal displacement and (b) vertical displacement. Z_0 = 15cm, L = 76cm, and t_{base} = 5cm *(42)*.

4.2. Employing SMA as Reinforcements

As shown in Figures 3 and 8, the temperature gradient through slab thickness results in significant end movements in concrete slabs. Such end movements causes several distresses, and resolving them has always been a top priority for design engineers. This study aims to find a solution by employing low-cost multifunctional materials as a candidate for both controlling such displacements and the reinforcement purposes. Incorporating low-cost SMAs into the old pavement design could be considered as a significant step toward using multifunctional materials in the next generations of the infrastructures. As shown in Figure 9, as temperature increases, SMA shrinks due to the phase transformation from martensite to austenite. This behavior of the SMA could be employed to control thermal expansion in a composite beam (shown in Figure 9), and eventually areas around the transverse joints in concrete pavements.

Martensite and austenite phases are thermodynamically favored at lower and higher temperatures, respectively. Since these structures have different lattice sizes and symmetry, cooling austenite into martensite introduces internal strain energy in the martensitic phase. To reduce this energy, the martensitic phase forms many twins called “self-accommodating twinning” and is the twinning version of geometrically necessary dislocations. Since the shape memory alloy is manufactured at a higher temperature and is usually engineered so that the martensitic phase is dominant at operating temperature to take advantage of the shape memory effect, SMAs “start” highly twinned. When the martensite is loaded, these self-accommodating twins provide an easy path for deformation. Applied stresses will de-twin the martensite, but all of the atoms stay in the same position relative to the nearby atoms; no atomic bonds are broken or reformed (as they would be by dislocation motion). Thus, when the temperature is raised and austenite becomes thermodynamically favored, all of the atoms rearrange to the austenite structure. This behavior, known as shape memory effect, is the key feature of the SMAs used in the current study. Moreover,

the corrosion resistance of the SMA could improve the long-term durability of the pavement. The actuation property of the SMAs has widely been employed for many engineering applications, as discussed before. However, the cost issues of using SMAs becomes critical for civil engineering structures, which are relatively larger than other engineering structures. To overcome this issue, Iron-based SMAs are chosen in the current study given the motivations of this work, the low cost of their constituents.

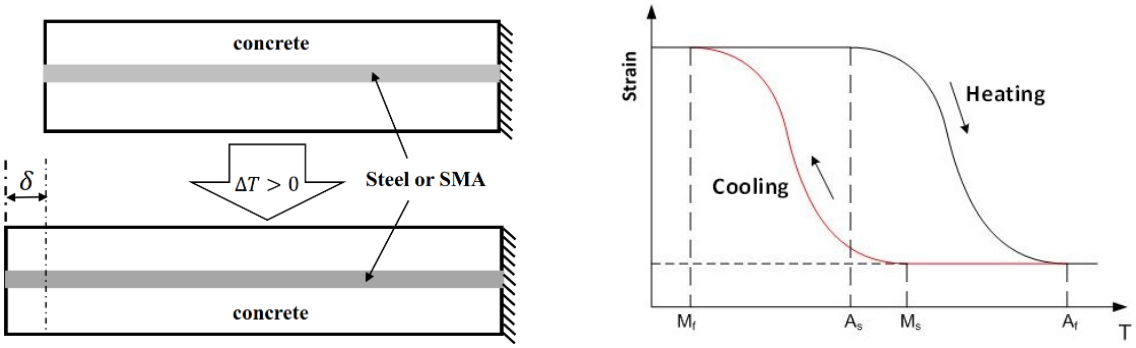

Figure 9. Controlling thermal expansion of the reinforced concrete using SMA.

5. ANALYSIS AND FINDINGS

5.1. Minimization of the Horizontal Displacement in Concrete Slabs

A system has been modeled in Abaqus *(52)* consisting of a concrete block with an embedded, pre-strained shape memory alloy (SMA) rod, as seen in Figure 10. Characterization of the SMA on this simple system undergoing thermal heating has been produced by iteratively altering a set of the SMA's material properties (max transformation strain, coefficient of thermal expansion, martensite and austenite stress influence coefficients, and volume fraction of SMA to concrete). The bounds for these design variables are given in Table 1.

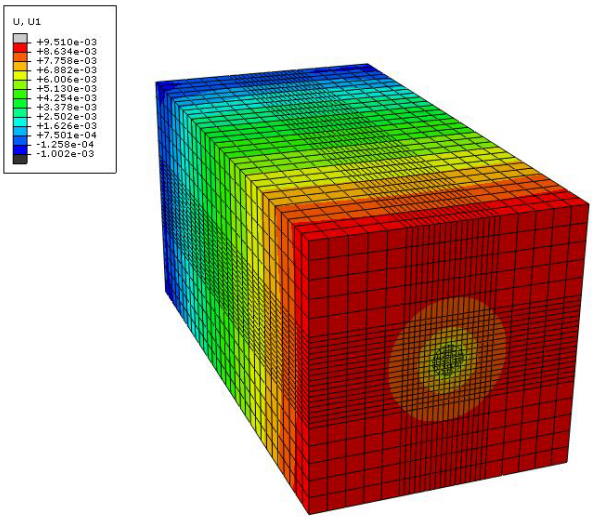

Figure 10. The concrete block and embedded SMA wire system as modeled in Abaqus, with axial displacement plotted over the body.

A three-level full factorial study is conducted using the given bounds and the system modeled. Each design is modeled twice, once undergoing a thermal expansion from 291 K to 316 K and another from 291 K to 266 K. Figure 11 shows change in temperature versus strain curves for the 243 FEA models evaluated, and a control case consisting of a simple thermal expansion calculation using the concrete's coefficient of thermal expansion. The open circles indicate the location where concrete damage occurs, evaluated by the max principal stress being greater than the fracture strength of concrete.

Table 1. Design variables and their bounds.

Design Variable	Minimum	Maximum
H_{max}^{t}	0.0034	0.0064
$\alpha\ (\frac{1}{K})$	$16.5E^{-6}$	$22.0E^{-6}$
$C_M\ (\frac{MPa}{K})$	0.53	3.1
$C_A\ (\frac{MPa}{K})$	0.53	3.1
$rod\ VF$	1%	5%

The most desirable designs in this analysis are those that have the lowest absolute value of strain and the largest temperature range before concrete damage occurs. The least desirable are those in

which the SMA actually deflects the concrete more than the control case. Figure 12 shows the design variables' effect on different objective functions. The martensitic stress influence coefficient (C_M) is shown to have a negligible effect on any objective function, which is to be expected considering the rod is starting fully martensite and phase-shifting into austenite. The austenite stress influence coefficient (C_A) is shown to contribute massively to the concrete stress, concrete deflection, and the temperature range. The rod volume fraction (Rod VF) is also shown to be a critical design variable, demonstrated by its effect on the concrete deflection.

A new system is currently being developed in Abaqus where the same concrete-SMA system described above is undergoing a thermal expansion cycle consisting of both heating and cooling to characterize the system in conditions that are more realistic. In addition to an updated thermal cycle, this system will also model the SMA as both an anchored rod and a cable. Once this system's development is completed, it will be used in the same full factorial study described above and again in a multi-objective optimization study. It should be mentioned that SMAs may not behave with stability across many thermal cycles (e.g., functional fatigue). However, the current study assumes that the SMA properties will not be fatigued as a result of temperature changes.

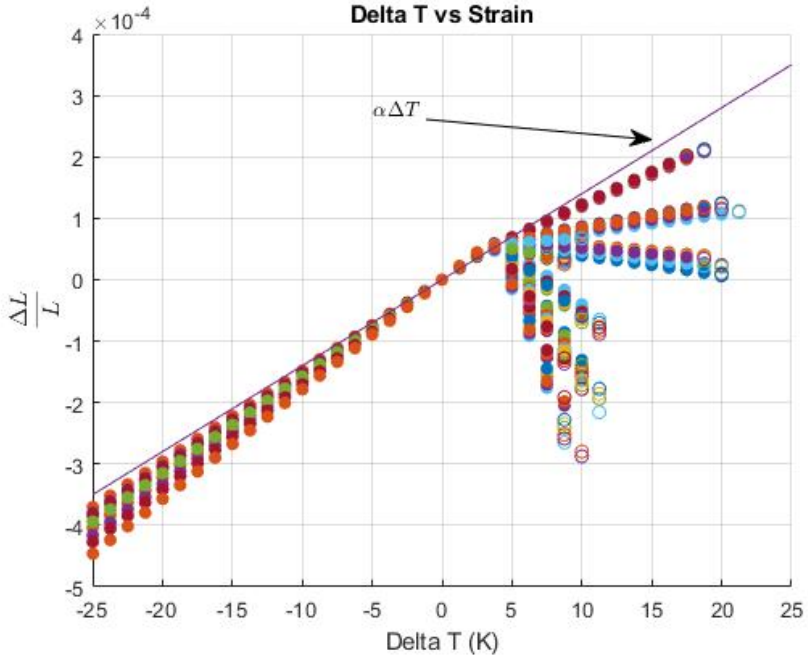

Figure 11. Temperature change versus strain curves for all designs evaluated.

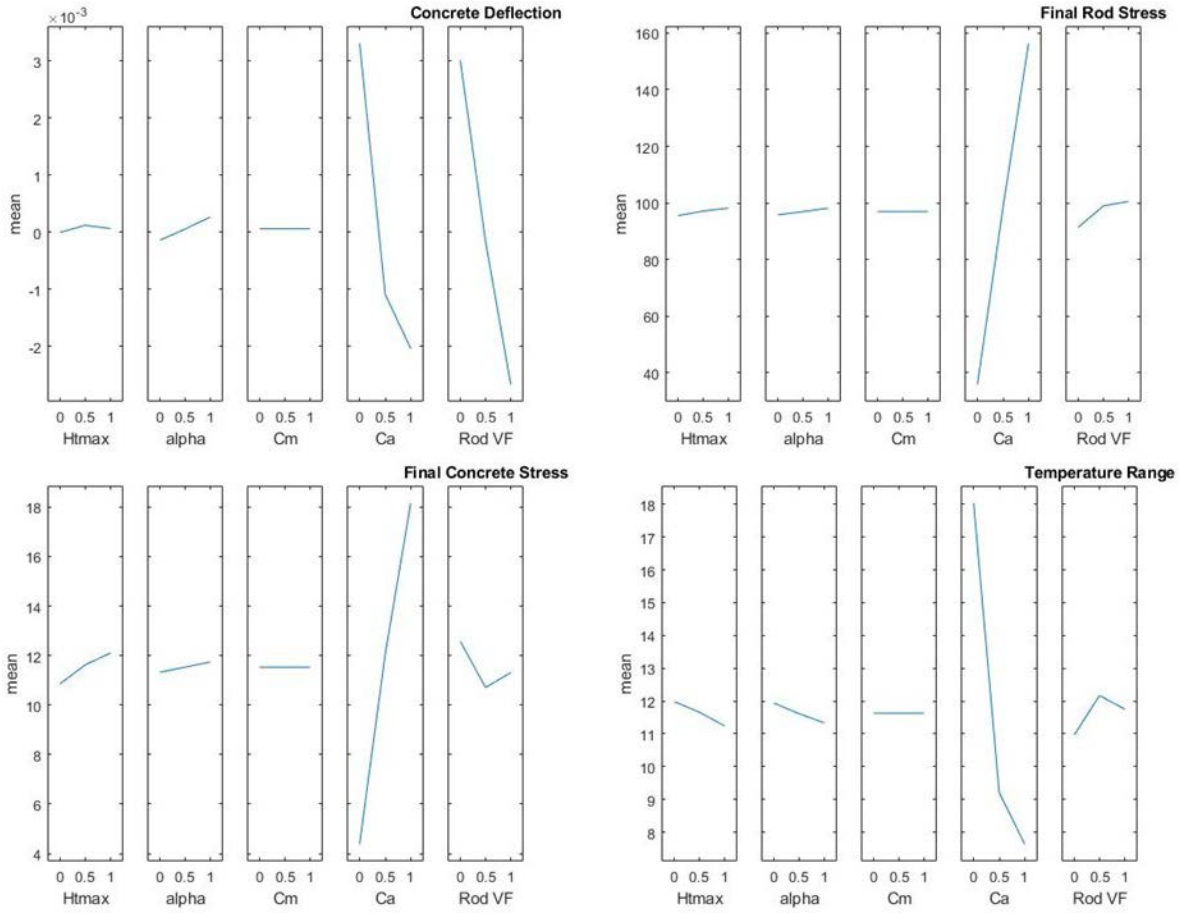

Figure 12. Factor effects plots of the design variables' effect on concrete deflection, final rod stress, final concrete stress, and the temperature range before concrete damage occurs.

5.2. Two-Dimensional FE Modeling of Concrete Slab Curling

Curling of the concrete slabs due to the temperature gradient throughout the slab thickness is a well-known example of distresses in transportation infrastructures due to thermal expansion. As a result, innovative solutions and strategies are needed to mitigate damage caused by the thermal expansion of transportation infrastructure. To enhance the longevity and safety of these structures, high-performance materials that address the issue of thermal expansion must be integrated into next generation designs. Understanding the behavior of concrete slabs experiencing temperature gradients, and the resulting "curling" phenomena has become the primary focus of this project, specifically, how shape memory alloys (SMA's) could be used to minimize this deflection, and thereby minimize cracking and erosion in concrete slabs.

Figure 6 shows a prism taken out of the middle of the edge of a typical CRCP structure in order to phenomenologically investigate temperature-induced end movements in concrete slabs. The deformation at the corners can be simulated by applying the corresponding boundary conditions. We have continued using Abaqus to model temperature induced deflection in concrete slabs and have created new models specifically to analyze the curling behavior. The model consists of three main parts: the sub-base, the concrete slab, and the embedded rod. The sub-base is encastered and serves to provide a structure that the concrete slab may be cohesively bonded to. The concrete slab itself is encastered on one end, allowing the rest of the structure to deform freely. The rod is

embedded into the concrete slab at a specified height, and when having SMA material properties, will serve to provide a counter-force to the force enacted by the temperature gradient. With fixed dimensions and material properties, the effects of temperature drop (which can be considered as a daily/ seasonal temperature changes) are obtained on horizontal and vertical displacements (point A in Figure 7). For the vertical displacement, called lift-off, the temperature change has the first-order effects and the impact of the other parameters. To start, a 2D model is constructed in Abaqus to see how changing the material properties of the embedded rod from steel to a magnetic SMA (MSMA) can change deflection at point A. The model will be constructed in 3D later and the effects of MSMA properties on the overall lift-off in the concrete slab will be evaluated comprehensively. Tables 2 and 3 list the geometrical parameters and the material properties used in the simulations.

In order to isolate the curling behavior, the model has constraints and boundary conditions such that both the sub-base and one end of the slab are encastered. This allows the concrete slab to respond freely to both the varying temperature loads and the cohesion force between the slab and base. However, to prevent over-constraining errors in the nodes that are a part of this encastered boundary condition as well as slab-base interaction, an analytical rigid back plate was used. Placed at the fixed end of the slab, this back plate was encastered while the slab and base were tied to the back plate. To ensure that the rod itself is capable of responding to forces, both external and internal (this will be important when SMA is used instead of steel), the rod and slab are created as two different parts. Then, using the "embedded region" constraint, the rod is placed internally within the slab.

Table 2. Geometrical parameters used in FE simulation.

Part	***Parameter***	***Description***	***Value***
Concrete Slab	t_0	Height	305 mm
	L	Length	4570 mm
Sub-base	t_{base}	Height	100 mm
	L	Length	4570 mm
Rod	d_s	Diameter	31 mm
	Z_0	Height from sub-base	167.5 mm

Table 3. Material properties used in FE simulation.

Material	*Parameter*	*Description*	*Value*
Concrete	σ_{ult}^{C}	Fracture strength	4 MPa
	E_C	Elastic modulus	35 GP
	ν_C	Poisson's ratio	0.2
	α_C	Coefficient of thermal expansion	1.6E-5 $^oC^{-1}$
	c_C	Specific heat	750 J/^{o}C
Cohesive Interaction	$\sigma_{MAX}^{Cohesive}$	Max cohesive strength	0.4 MPa
Steel Rod	E_s	Elastic modulus	200 GPa
	ν_S	Poisson's ratio	0.25
	α_S	Coefficient of thermal expansion	1.5E-5 $^oC^{-1}$
	c_S	Specific heat	490 J/^{o}C
SMA Rod	M_S	Martensite start temperature	310
	M_f	Martensite finish temperature	307
	A_S	Austenite start temperature	316
	A_f	Austenite finish temperature	325
	E_M	Martensite elastic modulus	50 GPa
	A_M	Austenite elastic modulus	90 GPa
	α_M	Martensitic coefficient of thermal expansion	1.65E-5 $^oC^{-1}$
	α_A	Austenitic coefficient of thermal expansion	1.65E-5 $^oC^{-1}$
	C_M	Martensitic stress influence coefficient	0.28 MPa/^{o}C
	C_A	Austenitic stress influence coefficient	0.28 MPa/^{o}C
	$H_{t,max}$	Maximum transformation strain	

An important factor to consider when analyzing curling within concrete slabs is the cohesion bond a slab creates when solidifying on top of the ground beneath it. In order to account for this, a surface to surface cohesive interaction property was utilized. This is distinct from cohesive elements, in that the interaction property uses only state-information from the interacting surfaces to determine the response. The maximum cohesive strength represents the maximum stress this bond can experience before being broken apart. Since the temperature gradient is from the cyclic temperature variations due to day-night cycles, the model has four steps corresponding to different times in the day. Each of these steps has a corresponding top-surface temperature and sub-layer temperatures (see Figure 13) that gradually progress as the day-night cycle unfolds. It should also be noted that in the Figures 14a-d, there is a 100 scaling factor to make the displacements visible.

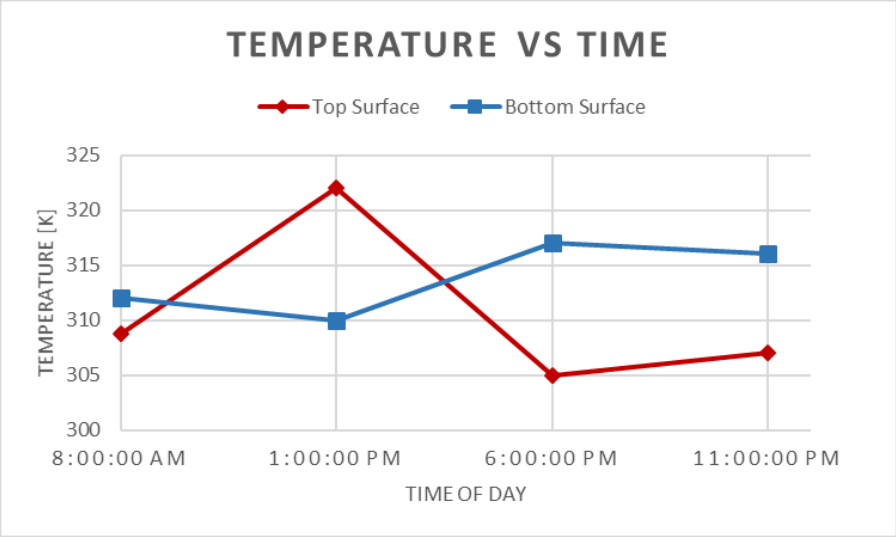

Figure 13. Defined temperature values for FE simulations.

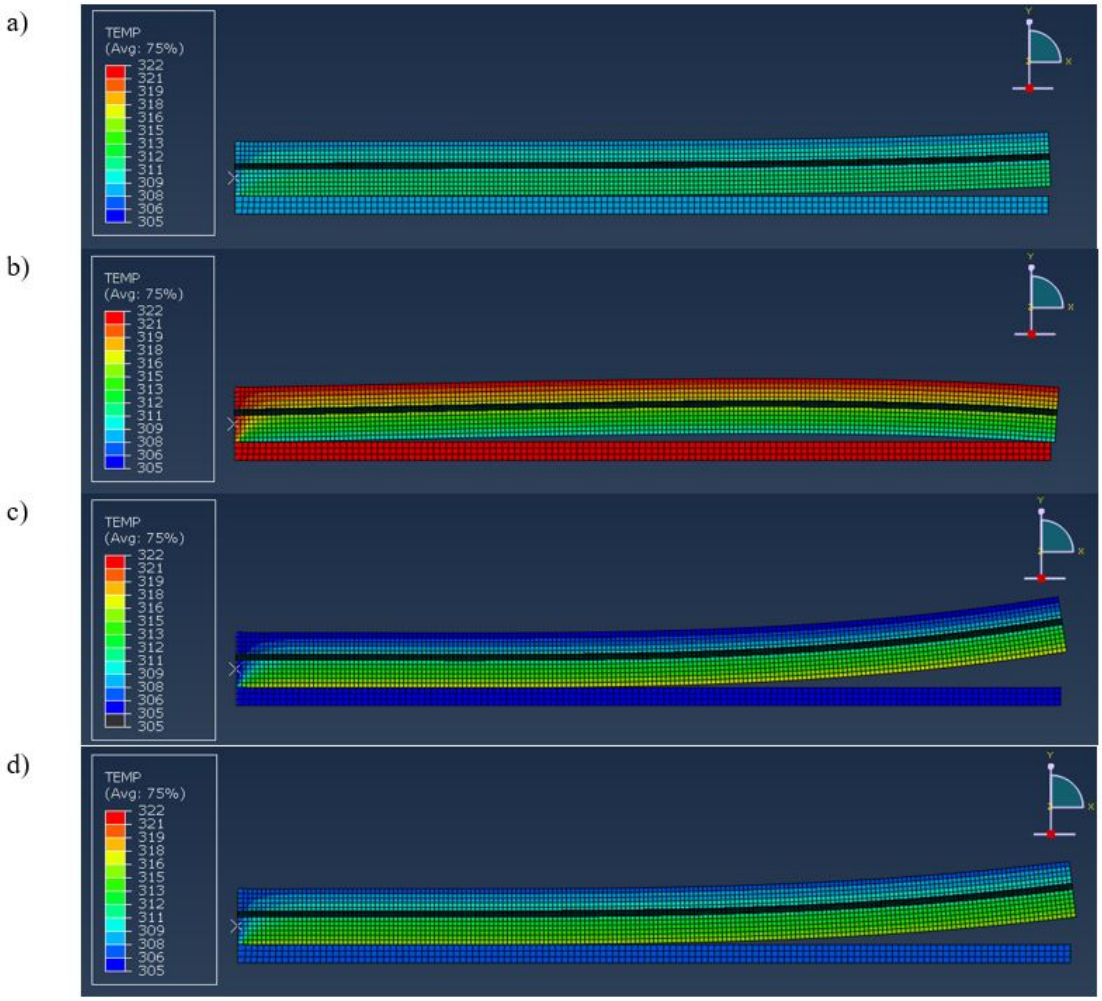

Figure 14. Deflection and temperature gradients for 1 Day: (a) 6 AM, (b) 12 AM, (c) 6 PM and (d) 10 PM.

As shown in Figures 15 and 16, the horizontal and vertical displacement at the slab's end (point A) alters as we replace the material properties of the bar from steel to an MSMA. However, the magnitude of these changes could be controlled by changing the material properties of the MSMA and the model should be optimized in this way, as discussed in Subsection 5.3.

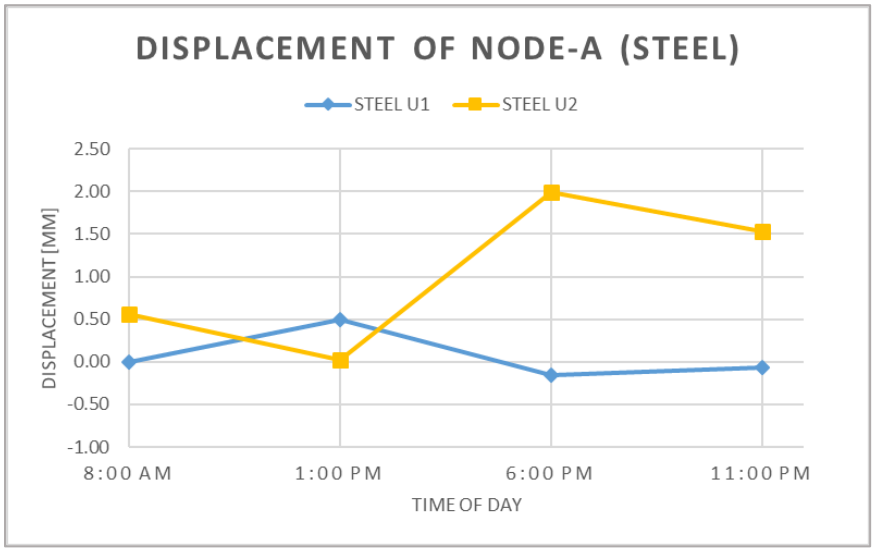

Figure 15. Deflection and temperature gradients for 1 Day using steel bar.

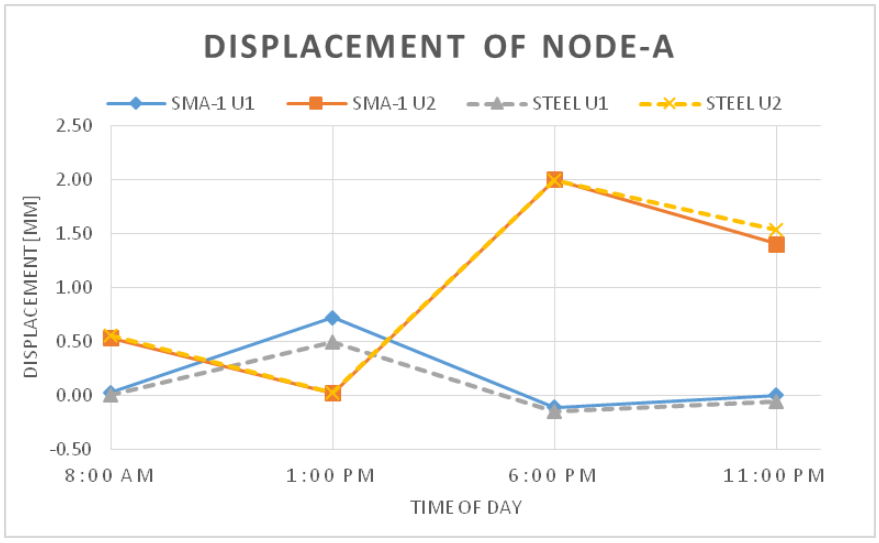

Figure 16. Deflection and temperature gradients for 1 Day, steel bar vs. SMA bar.

5.3. Three-Dimensional FE Modeling of Concrete Slab Curling

To better address the issue of curling in concrete slabs being controlled by using multifunctional materials, a 3D FE model is constructed to provide more realistic results than the 2D model. The 3-D Model is very similar to the 2-D, with a few variations. Since the simulation is very resource-intensive, the 3-D case was assumed to be symmetric about the YZ plane (shown in Figure 17) so that it was only necessary to simulate one half of the slab. This, as well as the remaining conditions imposed on the system, are described below.

One problem we initially faced with this model, was the rapid temperature variation when the model was initialized. Simply imposing temperature boundary conditions on the top and bottom surfaces and running it as a static problem means that Abaqus immediately attempts to solve for the equilibrium state. In the 2-D case, our User-Material script (UMAT) modeling SMA behavior was able to accomplish this, due to the 2-D case being considerably easier to compute. For the 3-D case, our UMAT was unable to solve for such a drastic and immediate temperature variation in our MSMA, so it was necessary to solve it as a dynamic problem. This allows for the temperature gradient to slowly grow through the concrete slab and MSMA. Making this change increased the runtime but allowed the simulation to come to convergence.

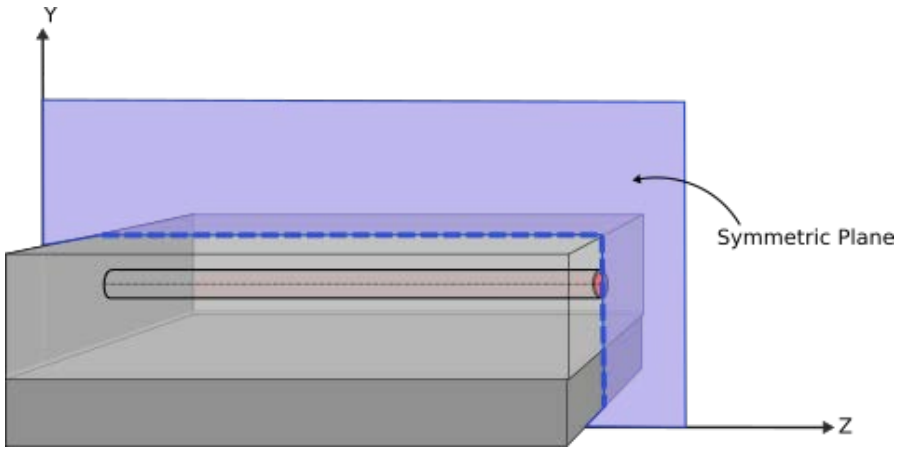

Figure 17. Symmetric plane for 3D modeling of the concrete slab curling.

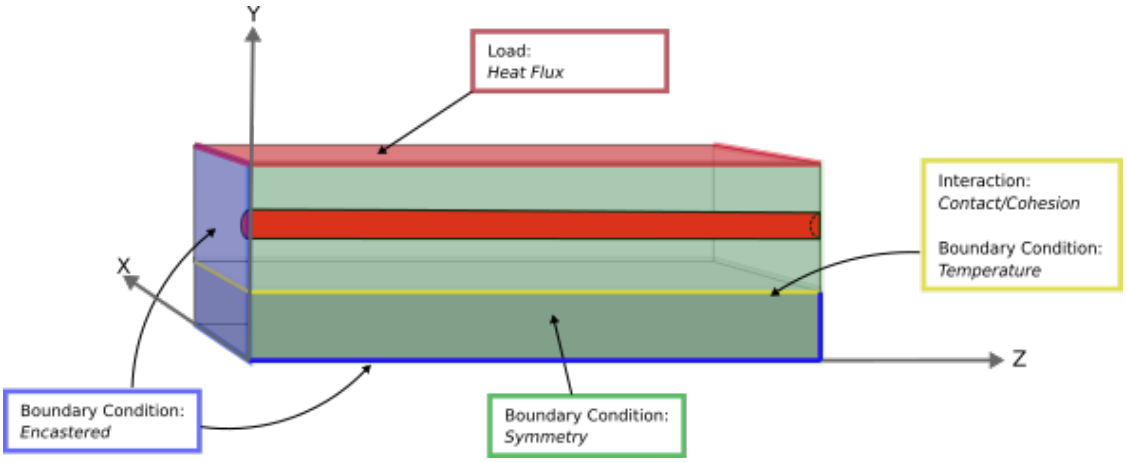

Figure 18. Regions of boundary conditions and loads in 3D FE modeling.

Symmetry: This boundary condition was applied to the face exposed due to the cut along the symmetric plane. It imposes that there is no movement in the X-direction, meaning it restricts movement along the X-axis and rotation along the Y-axis and Z-axis.

Encastered: Imposed on the back face of the slab and the exterior faces of the sub-layer, this boundary condition restricts all movement and rotation. Though this not be the case in real

applications, the purpose of this model is to study the curling behavior of the concrete. This boundary condition isolates this specific behavior and decreases the run-time of the simulation.

Contact/Cohesion: Between the surfaces of the slab and sub-layer, a contact interaction was defined. We used "hard" contact, meaning penetration was not allowed between the surface, and assumed the tangential behavior to be "frictionless." Though this may seem unrealistic and important for the behavior, the tangential behavior would be sufficiently captured by the cohesion between the two surfaces. This cohesive behavior was defined with normal and tangential material stiffness (Knn and Ktt) of 5 N/mm. Additionally, it was specified that after the maximum stress reached 0.4 MPa that this cohesion would be damaged and break (about 10% of the concrete tensile strength). It should be noted that for this model, surface-to-surface cohesion was utilized as opposed to cohesion elements. For this reason, it is included in the contact interaction.

Periodic Temperature Profiles: In order to fully capture the response to the thermal loads experienced in a day-night cycle, it is necessary to change the top and bottom surfaces of the slab to reflect those temperature changes. This was first done by having four different steps that each correspond to a different part of the day. Problems with this include unrealistic path-independent responses as well as immediate temperature variations that are unsolvable. The next iteration solved these by creating a heat flux load on the top surface of the slab, and allow the system to equilibrate accordingly. This solved the initial two problems but introduced two new problems of calculating appropriate heat flux to obtain a certain temperature and increasing run time significantly. We have solved all these problems by introducing a periodic amplitude and multiplying the initial temperature by this amplitude. Shown in Figure 19, are the amplitudes for the top and bottom surfaces.

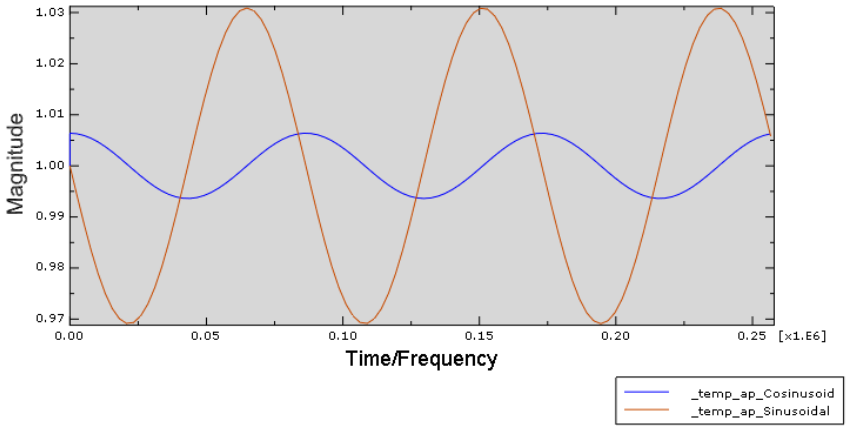

Figure 19. Abaqus periodic amplitude plot for temperature variations.

The period of these sinusoidal waves corresponds to one day in seconds and the magnitude is the percent increase/decrease we desire in surface temperature. These values are easily calculated if the initial temperature is specified. This method allows our simulation to capture the full temperature response, and to do it in a reasonable time span. The actual temperature values are shown in the results section below.

Moved Rod: In addition to different temperature boundary conditions, we also slightly changed the geometry from the conventional method. Previously, the rod's height from the base (z_0) was specified to be above the slabs midpoint (Figure 20). Now, the rod rests in the bottom half of the

slab, which allows for more efficient use of the curling load created by actuation of the SMA rod. All boundary conditions are illustrated in Figure 21 and the temperature variations on top, bottom, and the rod are shown in Figure 22.

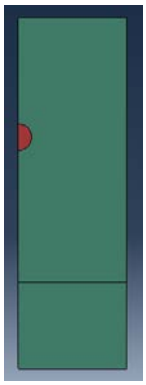

Figure 20. Positioning of the embedded rod.

Due to these changes, we have achieved a design that effectively mitigates the curling of concrete due to thermal cycling. In the plots below we have displayed the displacement of Node-A in both the vertical direction (normal to Sub-Layer) and in the longitudinal direction (along the length), as well as the temperature of the slab in different layers (Figure 22).

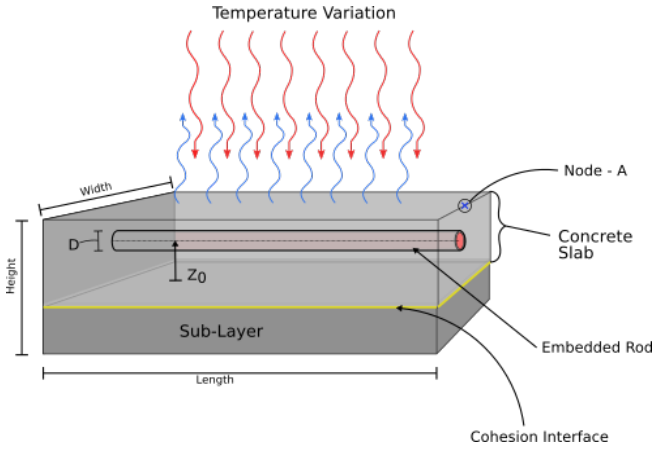

Figure 21. Visual explanation of parameters used for curling simulations.

The temperatures in slab's top, bottom, and the rod over 36 hours are shown in Figure 22 and the corresponding slab movements due to these temperature profiles are illustrated in Figure 23 at four parts of a day. It is seen that the concrete slab moves up and down during a day. The vertical and horizontal end movements in the concrete slab when using SMA bar are compared to the traditional case of using streel bar in Figures 24 and 25. It is found that using SMA bar can control these end movements significantly. The SMA bar starts to transform from martensite to the austenite around 4 pm as shown in Figures 26 and 27, resulting in significant changes in the vertical and horizontal end movements shown in Figure 24 and 25. However, the results obtained by the 3D FE simulations are needed to be optimized with respect to the SMA material properties and the geometrical parameters to achieve minimum displacements in the concrete slab due to the seasonal and daily temperature changes which are the next steps of the current research.

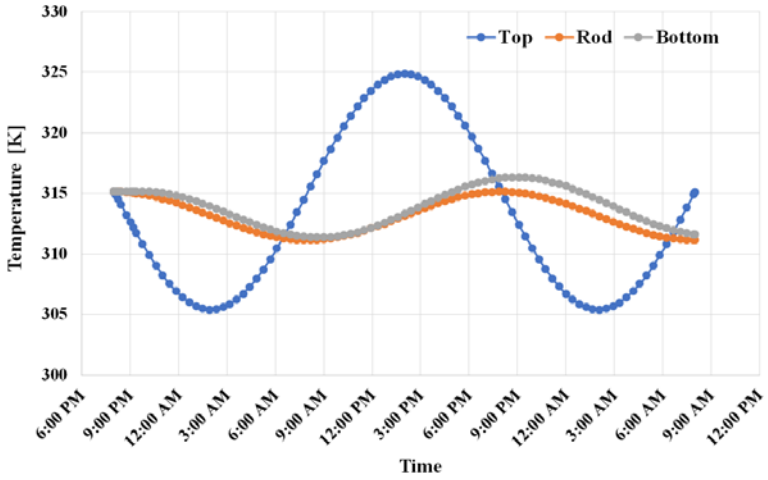

Figure 22. Plot showing the top, bottom, and rod temperature in the concrete slab over 36 hours.

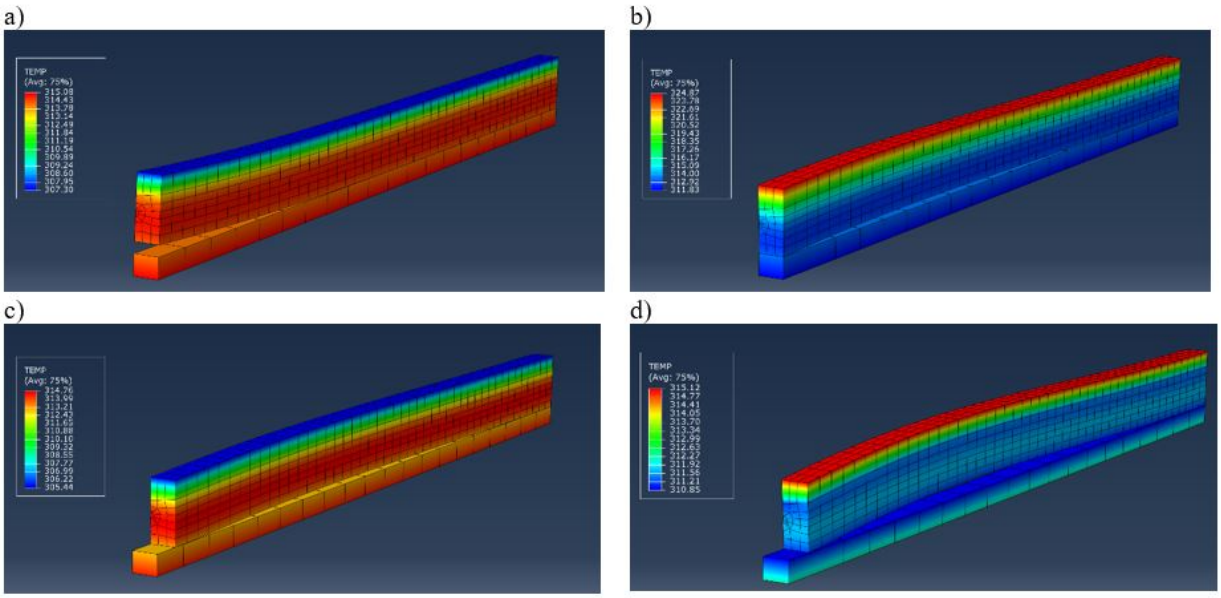

Figure 23. Slab displacements and the corresponding temperature profile plot after a) 3.5 hours (11:30 PM), b) 18 hours (2:00 PM), c) 30 hours (2:00 AM), d) 36 hours (8:00 AM).

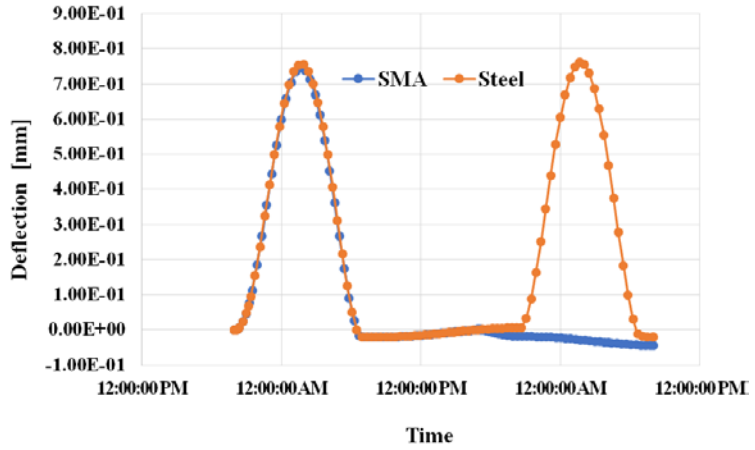

Figure 24. Vertical displacement of point A in the concrete slab over 36 hours.

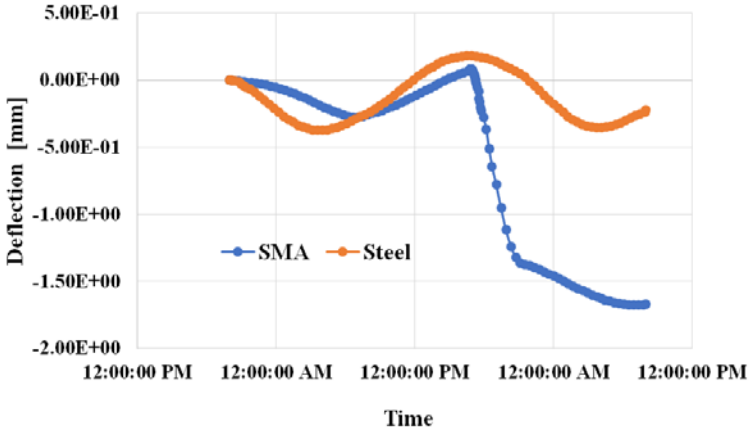

Figure 25. Horizontal displacement of point A in the concrete slab over 36 hours.

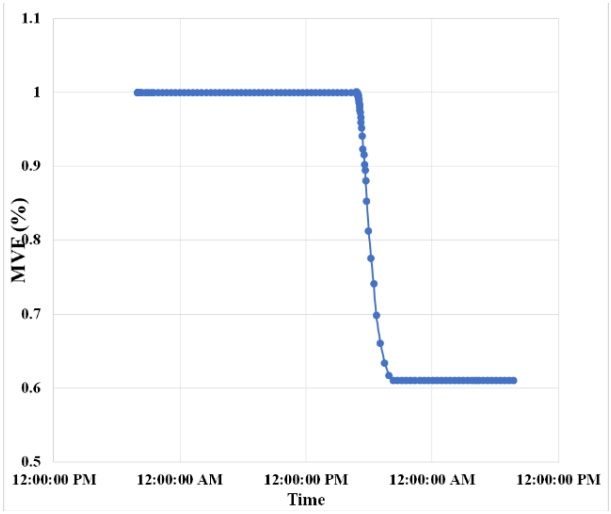

Figure 26. Evolution of the martensitic volume fraction in the SMA bar due to the daily temperature change.

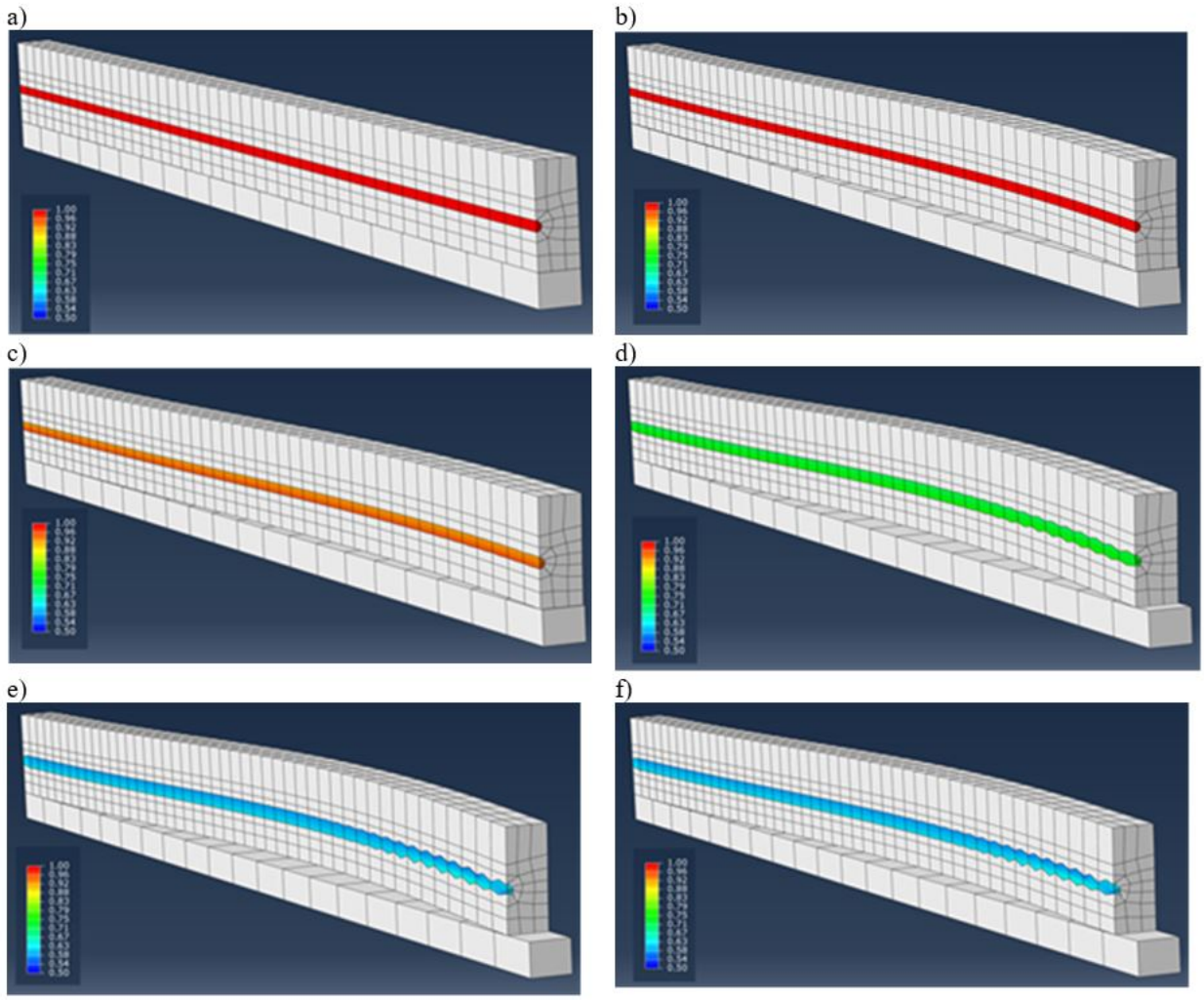

Figure 27. Martensitic volume fraction in embedded SMA rod at different time: (a) at initialization (8:00 PM), (b) after 16 hours (12:00 PM), (c) after 21 hours (5:00 PM), (d) after 23 hours (7:00 PM), (e) after 26 hours (10:00 PM), and (f) MVF after 36 hours (8:00 AM).

In order to further explore the most optimized version of the design, not only the radius size of the rod must be analyzed but also the location of the rod along with the slab thickness. The rod was positioned at different heights inside the concrete beam to observe the effects and changes over time when subjected to heating during the day. This will allow us to produce a beam that could potentially decrease the amount of deflection while using less material. This could also lead to fewer cracks being generated from the movement of the concrete leading to reduced overall curling affects.

Due to the nature of the finite element program running for long durations, the experimented values was limited. A total of 6 iterations was used to perform the experiment to find the best design. This low amount will not produce the most optimized design but it will point us in the right direction of what needs to be explored for future testing. The values for rod radius consisted of 165, 160, and 155 mm. These values were chosen since they are within the proximity of the previous optimized version. The values for the rod height was 157.5 and 177.5 mm. These values were chosen because the initial design called for a height of the rod from the sub base to be 167.5 mm.

The values were incremented in a small margin due to the unknown consequences of moving the rod height great distances. The beam was subjected to oscillating temperatures over a duration of 120,000 seconds (33 hours and 20 minutes) to simulate the temperature over the course of a day and a half. After this analysis, there can be further examinations for either larger or smaller changes from the original design. The corresponding slab displacements over time are illustrated in Figure 28.

Upon examining the results, it can be seen that the change in the rod produced little change as seen in Figure 29 and 30 throughout each iteration. The U1 direction (or x-direction) does not factor into decision making due to the negligible change in distance and change in deflection between each iteration. The U2 direction is of greater importance since it produces the most change. By looking at these results, the graphs for both U1 and U2 are very similar and have the same behaviors. The best determined design that had the least amount of deflection had a rod radius of 160 mm with a height below the sub base of 157.5 mm or with a height above the subbase of 177.5 mm. This result shows that the two values of the rod height would be the same if the rod was placed higher or lower along the z axis of the concrete slab. However, this might be due to the distance not being at a greater distance. The temperature could factor into the deflection when the distances are further apart and could generate other reactions. The temperature contours of the beam are displayed below to give a better understanding of how the beam changes throughout the day.

Since the differences between each iteration were very limited, we can safely say that the smaller radius value should be used in order to limit costs on manufacturing the SMA material. Further testing will need to be performed to determine if a smaller radius can be used at different locations to minimize the deflection while also minimizing the cost of manufacturing. When comparing the newfound optimized model to the older one (160 mm radius and 167.5 mm above sub base), it can be seen that the results are nearly the same. This shows that the lower radius can be used to limit the SMA material used in the structure.

Among the objectives of the current research was the design and characterization of multifunctional materials for the reduction of structural damage from thermal expansion. This task has extensively been investigated in the current research through finite element analysis. As the second objective, optimization of the topology and configuration of FeSMA materials have been conducted, and finally, as the last objective, the capabilities of the approach in designing the next generation of the smart infrastructures have been demonstrated through computational analysis. Indeed, further investigations are needed on experimental implementation of the Fe-SMA components in concrete structures. However, it strongly depends on the manufacturability of Fe-SMAs in large scales which is ongoing research.

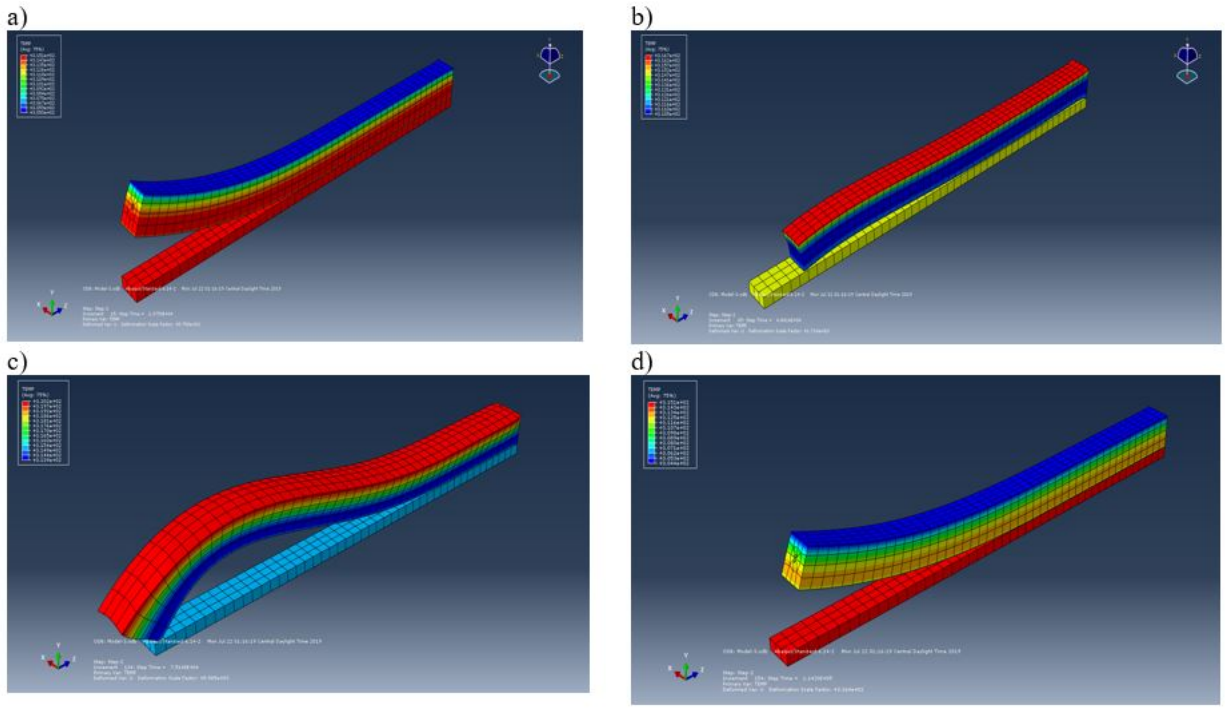

Figure 28. Temperature and movement over time: (a) After 4 hours, (b) After 13.5 hours, (c) After 21 hours, and (d) After 32 hours.

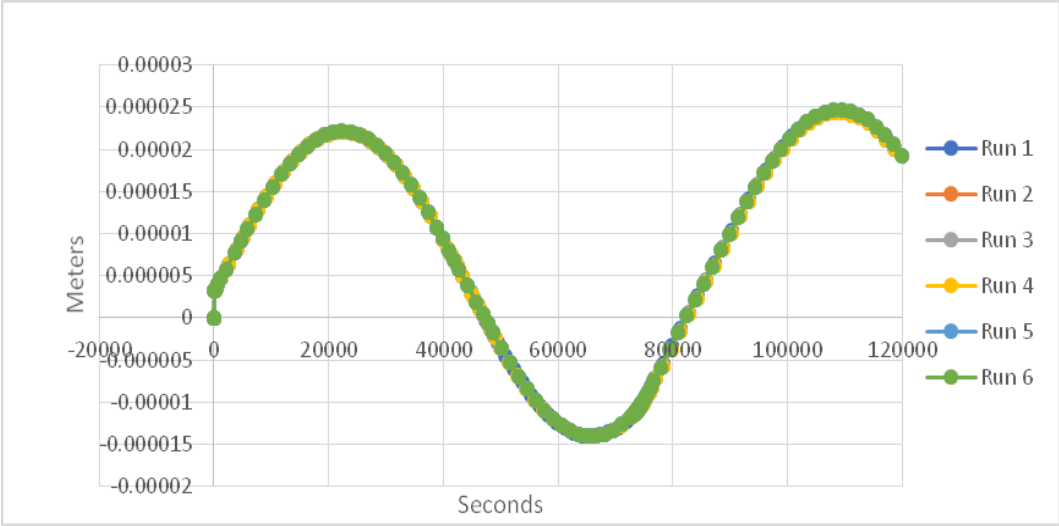

Figure 29. Tip deflection of each iteration in horizontal direction.

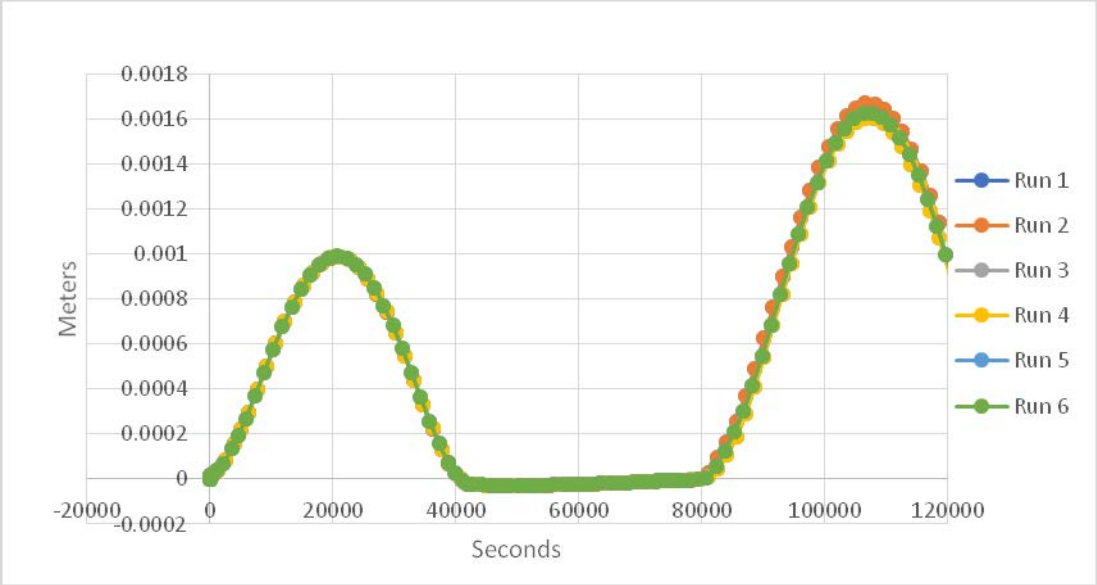

Figure 30. Tip deflection of each iteration in vertical direction.

6. CONCLUSIONS

The issue of thermal expansion in concrete structures was addressed in this research by replacing traditional steel rods with low-cost SMAs. The main idea of the project was to control the thermal expansion in concrete structures using multifunctional materials like shape memory alloys (as temperature increases, SMA shrinks due to the phase transformation from martensite to austenite. This feature of SMAs). To this end, curling of the concrete slabs due to the temperature gradient throughout the slab thickness, which is a well-known example of distresses in transportation infrastructures due to thermal expansion, was considered as a case to investigate. Through extensive two-dimensional and three-dimensional finite element simulations, it was found that SMAs can control the thermal expansion significantly.

The research topic explored in this report can be extended in many ways. The bond strength value for the concrete slab/subbase and SMA rod/concrete interfaces are more affected by the chemical bonds between two materials than their individual mechanical properties. The story is completely different for strong interfaces in which the interface crack kinks into one of the materials and therefore, the material property of the weaker material controls the interfacial fracture toughness. That means, a multiscale investigation is needed to understand the mechanism of bond failure for weak interfaces, which may not be necessary for strong interfaces. The output of the multiscale investigation of the concrete slab/ subbase and concrete slab/ reinforcing steel bar interfaces can be used for modification of the traction-separation constitutive law used in the current study. The SMA rod/ concrete corrosion may also affect the interfacial strength that can be considered as a future research.

The current research was mainly focused on the effects of environmental loads (temperature and moisture gradients) on the end movements in concrete pavements. The effect of traffic loads on the displacements in the concrete slab was not investigated in this study. This can also be considered as a future research topic. In fact, an in-service CRC pavement is subjected to both traffic and environmental loads simultaneously, which must be considered for design purposes. However, the primary source of slab lift-off and other distresses in CRC pavements are because of the environmental loads. Depending on main design goals, different properties can be defined and optimized for low-cost multifunctional materials used in concrete structures. It is worth mentioning that the fabrication of FE-SMA in large scales (for infrastructure applications) is an ongoing research and the current research only demonstrates a potential application of such multifunctional materials in next generation of infrastructures.

Regarding the position of the SMA rod, further testing will need to be performed with larger intervals to see how the distance from the subbase affects the concrete slab movements. This could provide further optimized results that could lead to a rod radius that is even more reduced which, in turn, could lower cost. However, the location of the SMA rod could be subjected to different temperature changes that could cause obscure results and produce ineffective structures. By exploring other uses of the concrete, a multi-use beam can be produced and can be used in everyday structures that might be subjected to different possible interactions with its environment. The results of this work could help to design smarter civil infrastructures incorporating multifunctional materials into the old civil engineering material.

REFERENCES

1. Mirsayar, M.M., K. Huang, and D.G. Zollinger. New approach to determining concrete slab lift-off by use of interfacial fracture mechanics concepts. *Transportation Research Record: Journal of the Transportation Research Board*, 2016 (2590), 10-17.

2. Takagi, T.A. Concept of intelligent materials. *Journal of Intelligent Material Systems and Structures*, 1990,1: 1149–1156.

3. Rogers, C.A. Intelligent material system—the dawn of new materials age. *Journal of Intelligent Material Systems and Structures*,1993, 4: 4–12.

4. Chen, Q. and C. Levy. Active vibration control of elastic beam by means of shape memory alloy layers. *Smart Materials and Structures*, 1996, 5: 400–406.

5. Janke, L., C. Czaderski, M. Motavalli, and J. Ruth . Applications of shape memory alloys in civil engineering structures – overview, limits and new ideas. *Materials and Structures*, 2005, 38: 578–592.

6. de Blonk, B.J., and D.C. Lagoudas. Actuation control of electrometric rods with embedded two-way shape memory alloy actuators. *Smart Materials and Structures*, 1998, 7: 771–783.

7. Cladera, A., E. Oller, and C. Ribas. Pilot experiences in application of shape memory alloys in structural concrete. *Journal of Materials in Civil Engineering*, 2013, 26(11): 04014084.

8. Wilde, K., P. Gardoni, and Y. Fujino. Base isolation system with shape memory alloy device for elevated highway bridges. *Engineering Structures*, 2000, 22: 222–229.

9. Cladera, A, B. Weber, C. Leinenbach, C. Czaderski, M. Shahverdi, and M. Motavalli. Iron-based shape memory alloys for civil engineering structures: an overview. *Construction and building materials*, 2014, 63: 281–293.

10. Buckle, J.G., and R.L. Mayes. Seismic isolation: History, application and performance—a world overview. *Earthquake Structures*, 1990, 6(2): 161–202.

11. Graesser, E.J., and F.A. Cozzarelli. Shape memory alloys as new materials for aseismic isolation. *ASCE—Journal of Engineering Mechanics*, 1991, 117(11): 2590–2608.

12. Czaderski, C., M. Shahverdi, R. Brönnimann, C. Leinenbach, and M. Motavalli. Feasibility of iron-based shape memory alloy strips for prestressed strengthening of concrete structures. *Construction and Building Materials*, 2014, 56: 94–105.

13. Shahverdi, M., C. Czaderski, P. Annen, and M. Motavalli. Strengthening of RC beams by iron-based shape memory alloy bars embedded in a shotcrete layer. *Engineering Structure*, 2016, 117: 263–273.

14. Billah, A.H.M.M., and A.M. Shahria. Plastic hinge length of shape memory alloy (SMA) reinforced concrete bridge pier. *Engineering Structure*, 2016, 117: 321–331.

15. Clark, P.W., I.D. Aiken, J.M. Kelly, M. Higashino, and R.A. Krumme. Experimental and analytical studies of shape memory alloy damper for structure control. In: Proceedings of Passive Damping, 1995.

16. Constantinou, C, and I.G. Tadjbakhsh. Hysteretic dampers in base isolation: random approach. *ASCE—Journal of Structure Engineering*, 1986, 22(2): 171–193.

17. Wilde, K, Y. Zheng, P. Gardoni, and Y. Fujino. Experimental and analytical study on shape memory alloy damper. In: SPIE—Proceedings of Smart Systems for Bridges, Structures, and Highways, 1998, 3325: 182–191.

18. Kajiwara, S. Characteristic features of shape memory effect and related transformation behavior in Fe-based alloys. *Materials Science and Engineering: A*, 1999, 273: 67-88.

19. Ariapour, A, D.D. Perovic, I. Yakubtsov. Shape-memory effect and strengthening mechanism in a Nb and N-doped Fe-Mn-Si-based alloy. *Metallurgical and Materials Transactions A*, 2001, 32(7): 1621-1628.

20. Hayashi, R., S.J. Murray, M. Marioni, S.M. Allen, and R.C. O'Handley. Magnetic and mechanical properties of FeNiCoTi magnetic shape memory alloy. *Sensors and Actuators A: Physical*, 2000, 81, 219–223.

21. Omori, T., K. Ando, M. Okano, X. Xu, Y. Tanaka, I. Ohnuma, R. Kainuma, and K. Ishida. Superelastic effect in polycrystalline ferrous alloys. *Science*, 2011, 333, 68.

22. Tanaka, Y., Y. Himuro, R. Kainuma, Y. Sutou, T. Omori, and K. Ishida. Ferrous polycrystalline shape-memory alloy showing huge superelasticity. *Science*, 2010, 327, 1488.

23. Ma, J., and I. Karaman. "Expanding the repertoire of shape memory alloys. *Science*, 2010, 327, 1468.

24. Monroe, J.A., D. Gehring, I. Karaman, R. Arroyave, D.W. Brown, and B. Clausen. Tailored thermal expansion alloys. *Acta Materialia*, 2016, 102: 333-341.

25. Monroe, J.A., I. Karaman, and R .Arroyave. U.S. Patent Application 2016, No. 15/217,594.

26. Monroe, J.A., I. Karaman, and R .Arroyave. U.S. Patent Application 2014, No. 14/897,904.

27. Highway Research Board. Continuously Reinforced Concrete Pavement. National Cooperative Highway Research Program Synthesis of Highway Practice 16, Washington D.C., 1973.

28. AASTHO. AASHTO Guide for the Design of Pavement Structures. American Association of State Highway and Transportation Officials, Washington D.C., 1986.

29. Nam JH. Early-age behavior of CRCP and its implications for long-term performance [Dissertation]. Austin, Texas: University of Texas at Austin, 2005.

30. Cha SW. Modeling of hydration process and analysis of thermal and hygral stresses in hardening concrete [Dissertation]. Seoul, Korea: Seoul National University, 1999.

31. Mehta PK, Monteiro PJM. Concrete: Microstructure, properties, and materials. Second Edition, the McGraw-Hill Companies, Inc., 1993.

32. Mindess S, Young JF. Concrete. New Jersey, USA: Prentice-Hall Inc.,1981.

33. Kosmatka SH, Panarese WC. Design and control of concrete mixtures. Illinois, USA: Portland Cement Association, 1988.

34. Samarai M, Popovics S, Malhotra, VM. Effect of high temperatures on the properties of hardened concrete. *Transportation Research Record: Journal of the Transportation Research Board* , 1983, 924.

35. Suh YC, Hankins K, McCullough BF. Early-age behavior of continuously reinforced concrete pavement and calibration of the failure prediction model in the CRCP-7 Program. Center for Transportation Research, The University of Texas at Austin, Report # 1244-3. 1992.

36. McCullough BF, Zolinger D, Dossey T. Evaluation of the performance of Texas pavements made with different coarse aggregates. Center for Transportation Research, The University of Texas at Austin, Report # 3925-1. 1999.

37. Polak MA. Effective stiffness model for reinforced concrete slabs. Journal of Structural Engineering. 1996; 122(9):1025-30.

38. Polak MA, Vecchio FJ. Nonlinear analysis of reinforced-concrete shells. Journal of Structural engineering. 1993; 119(12):3439-62.

39. Zhang J, Li VC. Influence of supporting base characteristics on shrinkage-induced stresses in concrete pavements. Journal of transportation engineering. 2001, 127(6):455-62.

40. Palmer, R.P. A mechanistic model for the prediction of stresses, strains, and displacements in continuously reinforced concrete pavements. [Dissertation]. College Station, Texas: Texas A&M University, 1988.

41. McCullough, B.F., and B.L. William. LTS Design of Continuously Reinforced Concrete Pavements. *Journal of the Highway Division, Proceedings of the ASCE*, 86, 1960.

42. Mirsayar M. On the Use of Interfacial Fracture Mechanics Approaches for Evaluation of the End Movement in Concrete Slabs. [Dissertation]. College Station, Texas: Texas A&M University, 2017.

43. Jeong, J.H., and D.G. Zollinger. Environmental effects on the behavior of jointed plain concrete pavements. *Journal of Transportation Engineering*, 2005, 131(2): 140-148.

44. Tseng, L.W., and J. Ma, B.C. Hornbuckle, I. Karaman, G.B. Thompson, Z.P. and Luo, Y.I. Chumlyakov. The effect of precipitates on the superelastic response of [100] oriented FeMnAlNi single crystals under compression. *Acta Materialia,* 2015, 97: 234-244.

45. Tseng, L.W., M. Vollmer, I. Karaman, T. Niendorf, and Y.I. Chumlyakov. Effect of grain size on the superelastic response in FeMnAlNi polycrystalline alloy under tension. *Scripta Materialia,* 2015, 125: 68-72.

46. Tseng, L.W., J. Ma, S.J. Wang, I. Karaman, M. Kaya, Z.P. Luo, and Y.I. Chumlyakov. Superelastic response of a single crystalline FeMnAlNi shape memory alloy under tension and compression. *Acta Materialia,* 2015, 89: 374-383.

47. Ma, J., B. Kockar, A. Evirgen, I. Karaman, Z.P. and Y.I. Luo. Chumlyakov. Shape Memory Behavior and Tension-Compression Asymmetry of a Novel FeNiCoAlTa Single Crystalline Shape Memory Alloy. *Acta Materialia*, 2012, 60: 2186.

48. Ozcan, H., J. Ma , S.J. Wang, I. Karaman, Y. Chumlyakov, J. Brown, and R.D. Noebe. Effects of cyclic heat treatment and aging on superelasticity in oligocrystalline Fe-Mn-Al-Ni shape memory alloy wires. *Scripta Materialia*, 2017, 134: 66-70.

49. Kim SM, Won M, McCullough BF. Development of a finite element program for continuously reinforced concrete pavements. Federal Highway Administration, Report # FHWA/TX-98/1758-S. 1997.

50. Kim SM, Won M, McCullough BF. Three dimensional nonlinear finite element analysis of continuously reinforced concrete pavements. Center for Transportation Research, The University of Texas at Austin, Report#1831-1. 2000.

51. William GW, Shoukry SN. 3D finite element analysis of temperature-induced stresses in dowel jointed concrete pavements. *International Journal of Geomechanics*, 2001, 1(3):291-307.

52. Abaqus. User's Manual Version 6.8. Providence, RI.: Habbit, Karlsson and Sorensen, Inc., 2008.

53. Lagoudas, D., D. Hartl, Y. Chemisky, L. Machado, and P. Popov. Constitutive Model for the Numerical Analysis of Phase Transformation in Polycrystalline Shape Memory Alloys. *International Journal of Plasticity*, 2012, 32–33: 155–183.